Journal of Dermatological Science 74 (2014) 116–124

Contents lists available at ScienceDirect

Journal of Dermatological Science

journal homepage: www.jdsjournal.com

# VEGF-A promotes IL-17A-producing γδ T cell accumulation in mouse skin and serves as a chemotactic factor for plasmacytoid dendritic cells

Takahiro Suzuki [a], Satoshi Hirakawa [a], Takatoshi Shimauchi [a], Taisuke Ito [a], Jun-ichi Sakabe [a], Michael Detmar [b], Yoshiki Tokura [a,*]

[a] Department of Dermatology, Hamamatsu University School of Medicine, Hamamatsu, Japan
[b] Institute of Pharmaceutical Sciences, Swiss Federal Institute of Technology, ETH Zurich, Zurich, Switzerland

ARTICLE INFO

*Article history:*
Received 11 September 2013
Received in revised form 27 December 2013
Accepted 27 December 2013

*Keywords:*
VEGF
IL-17
γδ T cell
Plasmacytoid dendritic cell
Chemotaxis
Psoriasis

ABSTRACT

*Background:* IL-17-producing $CD4^+$ T (Th17) cells and their cytokines, IL-17A and IL-22, are deeply involved in the pathogenesis of psoriasis by stimulating epidermal keratinocytes to proliferate and to produce cytokines/chemokines and vascular endothelial growth factor (VEGF)-A. Plasmacytoid dendritic cells (pDCs), infiltrating in psoriatic lesions, are known to exacerbate the Th17-mediated pathogenesis of psoriasis.

*Objective:* To address the initiative role of VEGF-A in the development of psoriasis and the pDC accumulation.

*Methods:* Numerical changes and VEGF receptor 1 (VEGFR1) and VEGFR2 expressions were investigated in skin-infiltrating T cells and pDCs of K14-VEGF-A transgenic (Tg) and wild type (WT) mice. The chemotactic properties of VEGF-A for purified splenic pDCs were also evaluated by real-time chemotaxis assay.

*Results:* By flow cytometry and immunohistochemistry, we observed that the number of dermal $IL\text{-}17A^+$ γδ T cells, but not $CD4^+$ T cells, was increased in VEGF-A Tg mice, suggesting that the main source of IL-17A was γδ T cells. Moreover, we identified pDCs as $440c^+$ cells by immunohistochemistry and as $PDCA\text{-}1^+B220^+$ cells by flow cytometry, and found that pDCs infiltrated at a higher frequency in VEGF-A Tg than WT mice. pDCs, but not γδ T cells, isolated from the skin expressed VEGFR1 and VEGFR2. Freshly isolated splenic pDCs expressed both receptors after 48-h cultivation. pDCs did not produce cytokines in response to VEGF-A, however, they had a strong velocity of chemotaxis toward VEGF-A at a comparable level to chemerin.

*Conclusions:* These findings suggest that VEGF-A functions as not only a downstream enhancer but also an upstream initiator by chemoattracting pDCs in psoriatic lesions.



## 1. Introduction

Recent accumulating evidence has demonstrated that psoriasis is mediated by interleukin (IL)-17-producing T helper (Th17) cells and their released IL-17 and IL-22 [1]. For maintenance of Th17 cells, IL-23 is essential and released from tumor necrosis factor-α (TNF-α) and inducible nitric oxide synthetase-producing inflammatory dendritic cells (DCs) [2]. The inflammatory DCs are activated *via* autocrine mechanism by virtue of TNF-α. Thus, the expression of IL-17, IL-22, IL-23, and TNF-α is elevated in psoriatic skin compared to normal skin [1,3]. This cytokine network has been proven by the therapeutic effectiveness of cytokine blocking biologics [4], including antibody therapies to TNF-α, IL-23/IL-12p40, and IL-17 or its receptors. It is noted that IL-17 and IL-22 are mainly produced by Th17 cells in human, but they may be derived from γδ T cells in mouse psoriatic or other inflammatory models [5–7].

IL-22 is the most effective cytokine for keratinocyte proliferation [8]. IL-17 and/or IL-22 are capable of stimulating keratinocytes to produce cytokines/chemokines and antimicrobial peptides [9]. Vascular endothelial growth factor (VEGF) is also produced by epidermal keratinocytes in synergistic stimulation with IL-17 and IL-22 [10]. Thus, proliferative keratinocytes in psoriatic skin are a major source of VEGFs [11], and VEGFs induce microvascular alterations in the dermal papillae essential for the development and persistence of the psoriatic lesions. Vasculature provides

* Corresponding author at: Department of Dermatology, Hamamatsu University School of Medicine, 1-20-1 Handayama, Higashi-ku, Hamamatsu 431-3192, Japan. Tel.: +81 53 435 2303; fax: +81 53 435 2368.
*E-mail addresses:* tokura@hama-med.ac.jp, tamaeo@hama-med.ac.jp (Y. Tokura).

0923-1811/$36.00 
http://dx.doi.org/10.1016/j.jdermsci.2013.12.013

cellular and tissue nutrition to hyperplastic keratinocytes and promotes inflammatory cell migration [12].

VEGFs constitute a family of six polypeptides, VEGF-A, -B, -C, -D, -E and PlGF, which regulate blood and lymphatic vessel development. VEGFs specifically bind to VEGFR1, 2 and 3, and to coreceptor neuropilins (Nrps) [13]. VEGF-A, a major regulator for angiogenesis, binds and activates two tyrosine kinase receptors, VEGFR1 and VEGFR2. While VEGFR2 has strong tyrosine kinase activity and transduces the major signals for angiogenesis, VEGFR1 plays dual roles, a negative role in embryonic angiogenesis and a positive role in adulthood in a tyrosine kinase-dependent manner [14]. VEGFR1 is expressed not only in endothelial cells but also in macrophage/monocyte-lineage cells [15] and even leukemic cells [16], and promotes tumor growth, metastasis, and inflammation [15]. Therefore, VEGFR1 is also a therapeutic target for human diseases.

In addition to Th17 cells, inflammatory DCs, and their cytokines, plasmacytoid DCs (pDC) are deeply involved in the pathogenesis of psoriasis [17,18]. pDCs are maturated from hematopoietic progenitor cells and migrate to the skin in various pathological conditions [19]. Upon stimulation with toll-like receptor ligands [20] and antimicrobial peptide-self DNA complex [21], pDCs produce type 1 interferon (IFN) such as IFN-α. Although the target cells of IFN-α remain to be elucidated, pDC-derived IFN-α is thought to promote the Th17- or Th1-based cascade of psoriasis.

Considering that VEGF is not only an angiogenetic factor but also an inflammatory promotor, it is possible that keratinocyte-derived VEGF stimulates pDCs that infiltrate in the upper dermis. The aforementioned finding that monocyte/macrophage-lineage cells express VEGFR1 further supports this possibility. We therefore sought to investigate the role of VEGF-A for the activation of pDCs. We used K14-VEGF-A transgenic mice (Tg) [22,23], which exhibit spontaneous skin lesions resembling psoriasis [24,25]. Moreover, we studied *in vitro* the ability of VEGF-A to chemoattract freshly isolated pDCs.

## 2. Materials and methods

### 2.1. Mice

The K14-VEGF transgenic mice over-expressing VEGF-A164 in the epidermal basal layer were generated on FVB background by inserting an expression cassette containing the human K14 promoter and the gene encoding murine VEGF-A164 using the pronuclear microinjection technique [22]. The K14 promoter is expressed specifically in the basal layer of stratified squamous epithelium and controls expression of VEGF in the transgene construct [26,27]. Homozygous K14-VEGF mice were used in this study and wild type (WT) FVB mice were included as control groups. Female FVB/N JCL mice, 8 weeks of age, were purchased from CLEA Japan Inc. (Tokyo, Japan) and were maintained in specific pathogen-free conditions according to the guidelines of the Institute of Laboratory Animal Resources of Hamamatsu University School of Medicine. All animal experiments were approved by the Institution Animal Care and Using Committee.

### 2.2. Western blot analysis

We used skin samples from 8-week-old female mice for Western blotting. We pulverized skin in protein extraction buffer (100 mM phenylmethylsulfonyl fluoride, complete mini EDTA-free protease inhibitor cocktail 1 tablet) with Ultra-Turrax (IKA-Werke GmbH & Co. KG, Staufen, Germany). The homogenized tissues were disrupted by sonication. Cell lysates were centrifuged at 15,000 × *g*, and the supernatants were collected into fresh tubes. Then, 4× SDS buffer with 0.1 mol/L 2-mercaptoethanol was added to samples, which were boiled for 5 min at 95 °C. The extracts (30 μg) were separated by 20% SDS-PAGE and electroblotted onto polyvinylidene difluoride (PVDF) membranes (Bio-Rad Laboratories, Hercules, CA). After electroblotting, PVDF membranes were incubated with rabbit polyclonal antibodies to anti-mouse IL-17 (1:2000; Abcam, Cambridge, MA), goat polyclonal antibodies to anti-mouse IL-23p19 (1:1000; R&D, Minneapolis, MN), or β-actin (1:1000; Cell Signaling Technology, Danvers, MA), and the reaction was detected with horseradish peroxidase–conjugated goat anti-rabbit IgG (1:3000; Bio-Rad) or horseradish peroxidase–conjugated rabbit anti-goat IgG (1:1000; R&D). The signal was detected using an ECL Plus Western blot detection system (GE Healthcare, Piscataway, NJ).

### 2.3. Immunohistochemistry

Abdominal skin of mice was fixed in 4% paraformaldehyde for 10 min. Five μm paraffin-embedded tissue sections were first deparaffinized and dehydrated. Endogenous peroxidase activity was quenched by incubating the slides in a solution of 700 μl $H_2O_2$ (30%). The sections were incubated with primary antibody against mouse IL-17 (1:100; Abcam) and antibody against CCL20 (1:30, Abcam) at room temperature for 60 min. The slides were washed in Tris-buffered saline (TBS) and incubated with the peroxidase-conjugated affinipure goat anti-rabbit IgG (Jackson ImmunoResearch, West Grove, PA) at room temperature for 30 min. The slides were washed with TBS three times and incubated with diamino-benzidine-tetrahydrochloride (DAB) as substrate and counterstained with hematoxylin.

### 2.4. Immunofluorescence microscopy

Abdominal skin was embedded in OCT compound and snap-frozen. Cryostat sections were immunostained with anti-IL-17 (Abcam), anti-CCR6 (R&D), anti- SIGLEC H mAb (440c; Abcam), and anti-mouse CD11c mAb (Biolegend, San Diego, CA). The respective secondary antibodies were labeled with Alexa 488 or 594 (Molecular Probes, Eugene, OR). Nuclei were counterstained with 4′,6′-diamidino-2-phenylindole (DAPI) (Molecular Probes). Sections were examined, and digital images were captured using the Olympus FluoView™ FV1000 confocal laser scanning microscope (Tokyo, Japan). For pDCs, an immunohistochemical staining for 440c, known as a pDC marker [28], was performed in sections.

### 2.5. Flow cytometry

The following monoclonal antibodies (mAbs) were employed: phycoerythrin (PE)-labeled anti-mouse IL-17A, CD4, TCRγ/δ and B220 mAbs (all from Biolegend), Alexa Fluor 488-conjugated anti-mouse VEGFR1 mAb (Flt-1; R&D), FITC (fluorescein isothiocyanate)-labeled anti-mouse VEGFR2 mAb (Flk-1; BD PharMingen, San Jose, CA), and anti-neuropilin 1 (R&D), allophycocyanin (APC)-labeled anti-mouse PDCA-1 mAb (CD317; Biolegend), and PE-Cyanin7 (PE-Cy7)-labeled anti-mouse CD11c mAb (BD PharMingen). All mAbs were used at 1–5 $\mu g/10^6$ cells, and incubation was performed for 30 min at 4 °C, followed by two washes in phosphate-buffered saline (PBS, pH 7.4) supplemented with 5% fetal calf serum (FCS) and 0.02% sodium azide. Non-specific stains were performed with the adequate same-class immunoglobulin for specific mAb. Fluorescent profiles were generated using FACSCanto II (BD). Cells were first incubated with anti-mouse Fcγ II/III receptor mAb for 10 min to prevent non-specific binding of the subsequent reagents to Fc receptors. 7-Amino-actinomycin D (7-AAD) was added to exclude dead cells.

### 2.6. Isolation of skin-infiltrating cells, lymph node cells, and peripheral blood mononuclear cells

Skin sheets from mouse ears were separated from cartilage with forceps and incubated in PBS with 1% bovine serum albumin (BSA) containing collagenase I and collagenase II (Liberase TL Research Grade; Roche, Indianapolis, IN) for 10 min at 37 °C with dermal side down to separate epidermal sheets from dermal sheets. After both epidermis and dermis were minced, cells were then filtered through a 70-μm nylon mesh and washed before use. Fresh lymph nodes obtained from mice were minced with a scalpel, pipetted repeatedly in PBS, and strained through a 40-μm mesh to obtain a single-cell suspension. For peripheral blood cells, erythrocytes were lysed by incubating in lysis buffer (BD PharMingen) for 3 min and washed.

### 2.7. Isolation and culture of splenic pDCs and CD11c$^+$ DCs

Spleens freshly taken from mice were minced with a scalpel, pipetted repeatedly in PBS, and strained through a 40-μm mesh to obtain a single cell suspension. Erythrocytes were lysed by incubating in lysis buffer for 3 min and washed. Splenic pDCs were purified by negative selection using a MACS Plasmacytoid Dendritic Cell Isolation Kit II. Splenic CD11c$^+$ cells were purified by positive selection using a Magnetic Activated Cell Sorter with anti-mouse CD11c mAb (MACS; Miltenyi Biotec K.K. Tokyo, Japan). Splenic DCs were cultured at $1 \times 10^5$ cells/ml in 96-well plates. For the receptor expression study, they were cultured for 48 h in 200 μl complete RPMI 1640 (Sigma–Aldrich, St Louis, MO) containing 10% heat-inactivated FCS, $5 \times 10^{-5}$ M 2-mercaptoethanol, 2 mM L-glutamine, 25 mM HEPES, 1 mM non-essential amino acids, 1 mM sodium pyruvate, 100 units/ml penicillin and 100 μg/ml streptomycin.

### 2.8. ELISAs for IFN-α and TNF-α

pDCs were cultured at $1 \times 10^5$ cells/ml in complete RPMI 1640 for 48 h with the following maintenance factors: 5 μg/ml CD40L trimer (R&D), 2.5 μg/ml recombinant murine GM-CSF (R&D), 200 ng/ml recombinant human Flt-3 Ligand (R&D), and 20 ng/ml murine IL-3. Cultures were incubated at 37 °C in a humidified atmosphere and 0.1–100 ng/ml of recombinant mouse VEGF 164 (R&D) were added at the beginning of culture. As positive control, 10 μg/ml phosphorothioate-modified oligodeoxynucleotides (ODN) CpG motifs 1826 (InvivoGen, San Diego, CA) was used.

### 2.9. Chemotaxis assay

The chemotaxis of DCs was measured using an EZ-TAXIScan system according to the manufacturer's protocol (Effector Cell Institute, Kanagawa, Japan), an optically accessible horizontal chemotaxis apparatus, *via* a charge-coupled device camera (GE Healthcare, Tokyo, Japan) [29]. As chemotactic factors, the assay included 100 ng/ml (optimal for pDCs) or 250 ng/ml (CD11c$^+$ DCs) of recombinant mouse VEGF 164 (R&D, MN) and 500 μg/ml recombinant chemerin (R&D, MN). All cell suspensions and chemokine dilutions were made in complete RPMI 1640. After 60 min, the number of sorted cells that migrated toward VEGF front chamber in a straightforward manner was counted using an Image J. The cells that reached the upper chamber were preferentially considered. For blockade of interaction between VEGF-A and VEGF receptors, VEGFR1, VEGFR2 and Nrp1 neutralization was performed. pDCs isolated from splenocytes were preincubated with 10 μg/ml of antibodies to VEGFR1 [30], VEGFR2 [30], or Nrp1[31] (R&D) for 60 min at 37 °C.

### 2.10. Statistical analysis

Student's *t* test (two groups) or Kruskal–Wallis nonparametric test (more than three groups) was employed to determine statistical differences among means. *Post hoc* comparisons used Bonferroni-corrected Mann–Whitney *U* tests.

## 3. Results

### 3.1. Skin infiltration of IL-17-producing γδ T cells in VEGF-A Tg mice

We first characterized skin-infiltrating cells in VEGF-A Tg mice whose keratinocytes produce a high amount of VEGF-A. In accordance with the previous observation [25], skin samples from abdominal skin of 8-week-old VEGF Tg mice exhibited higher expressions of IL-17A and IL-23p19 than those of WT mice by Western blot analysis (Fig. 1A). This indicates that IL-23, a crucial cytokine for maintenance of Th17 cells, is elevated as well as IL-17A in this mouse model of psoriasis. Next, abdominal skin specimens were immunohistochemically stained with anti-IL-17A antibodies. The number of positive cells was expressed as cell number/high power field (HPF). The IL-17$^+$ lymphocyte frequency was enhanced by tape-stripping. A significantly higher number of IL-17$^+$ lymphocytes infiltrated in VEGF-A Tg mice than in WT mice (Fig. 1B).

In human psoriasis, the main producer of IL-17 is CD4$^+$ T cell, namely Th17 cell. However, several murine experimental systems for inflammatory conditions have disclosed that IL-17 is substantially released by γδ T cells [5–7]. We isolated skin-infiltrating cells from inflamed earlobes of 16-week VEGF-A Tg mice and performed flow cytometric analysis by intracellular IL-17A staining and surface γδTCR or CD4 staining. In a representative experiment (10 mice collectively analyzed), 25.3% of the gated fraction of γδ TCR$^+$ T cells had IL-17A in the cytoplasm, while a minimal percentage (0.5%) of CD4$^+$ T cells bore IL-17A (Fig. 2A). γδ TCR$^+$ T cells were double negative for CD4 and CD8 (data not shown). When 31 Tg mice and 19 WT mice were collectively analyzed, the percentage of IL-17A$^+$ γδ T cells in VEGF-A Tg mice was twice or more higher than that in WT mice, but IL-17$^+$ CD4$^+$ T cells were not increased compared to WT mice (Fig. 2B). Thus, γδ T cells were the major source of IL-17A in VEGF-A Tg mice.

We also compared IL-17$^+$ γδ T cell frequencies in the lymph nodes and peripheral blood of VEGF-A Tg mice. The percentages of IL-17$^+$ cells in γδ T cells were 26.8% in the skin, 2.0% in the lymph nodes, and 0.002% in the peripheral blood, suggesting preferential infiltration of IL-17$^+$ γδ T cells in the skin.

To address the mechanism underlying γδ T cell accumulation, the abdominal skin sections from 8-week VEGF-A Tg and WT mice were stained for chemokine receptor CCR6 and its ligand CCL20, which regulate migration of Th17 and γδ T cells. CCL20 was expressed in dermal fibroblasts, and its expression was increased in the tape-stripped VEGF-A Tg mice (Fig. 3A). By double-staining for CCR6 and γδ TCR, dermal-infiltrating γδ T cells bore its receptor CCR6, and their number was high in VEGF-A Tg mice (Fig. 3B). It is possible that VEGF-A mediates CCL20 expression *via* as yet unknown mechanism in fibroblasts and leads to γδT cell accumulation.

### 3.2. Skin infiltration of pDCs in VEGF-A Tg mice

The infiltrate of pDCs, as assessed by 440c immunoreactivity, was examined along with CD11c$^+$ DCs in the abdominal skin of 8-week VEGF-A Tg mice. 440c$^+$ cells infiltrated in the upper dermis at a higher frequency in VEGF Tg mice than in WT mice (Fig. 4A). The number of 440c$^+$ pDCs in VEGF-A Tg mice was three times of that in WT mice (Fig. 4B). CD11c$^+$ DCs were also increased in VEGF-A Tg mice more than twice of that in WT mice.

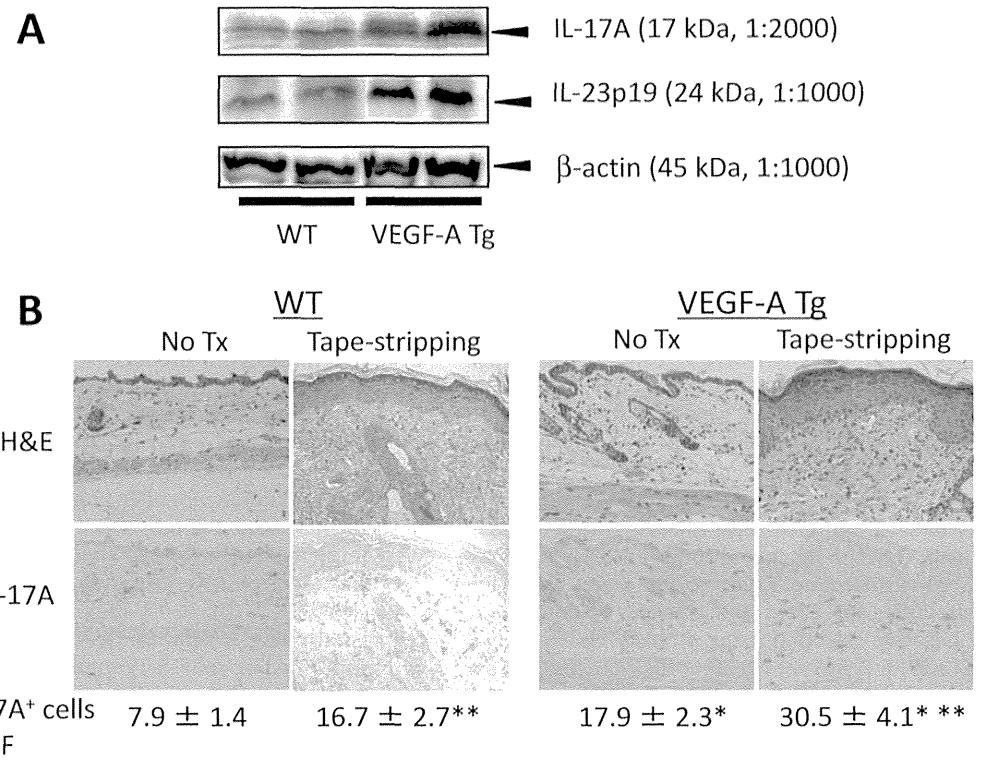


**Fig. 1.** IL-17A and IL-23p19 protein expressions and IL-17A$^+$ cell infiltration in abdominal skin of VEGF-A Tg mice. (A) Western blot analysis of abdominal skin specimens taken from 8-week-old VEGF-A Tg mice and WT mice. The expression levels of IL-17A and IL-23p19 were examined in parallel with that of β-actin. Parentheses indicate the molecular weight and the dilution of primary antibody. (B) Immunohistochemical study of IL-17A$^+$ cells in abdominal skin of VEGF-A Tg and WT mice tape-stripped or non-treated. The number indicates the mean ± SD ($n$ = 10) of IL-17$^+$ cells/HPF. *$P < 0.001$, compared with the corresponding WT mice. **$P < 0.001$, compared with the corresponding non-tape-stripped mice.

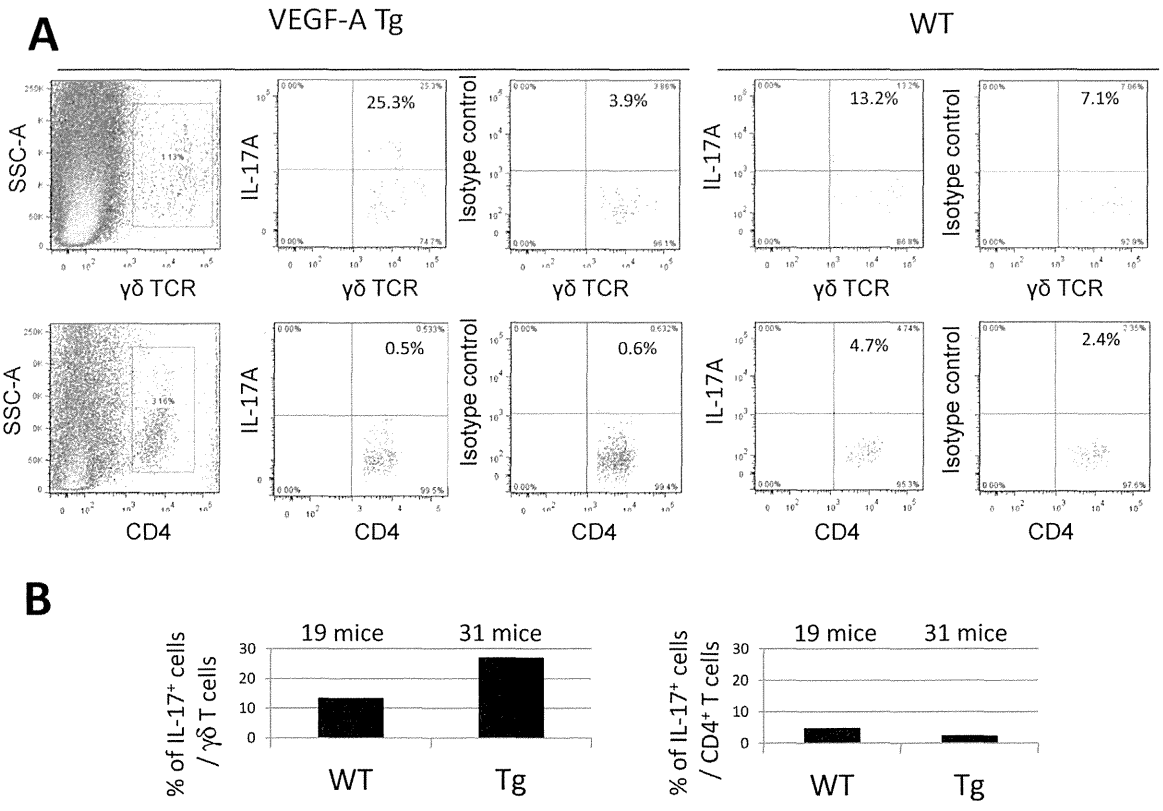


**Fig. 2.** IL-17$^+$ γδ T cells and CD4$^+$ T cells isolated from inflamed ear skin of VEGF-A Tg mice and normal-appearing ear skin of WT mice. (A) Flow cytometric analysis of skin-infiltrating cells from ears of 16-week-old VEGF-A Tg mice (10 mice collectively analyzed) and WT mice (10 mice collectively analyzed). Skin-infiltrating cells were isolated by collagenase treatment and were subjected to intracellular IL-17A staining and surface γδ TCR or CD4 staining. Representative flow cytometric data are shown. (B) Percentage of IL-17$^+$ cells in γδ T cells and IL-17$^+$ cells in CD4$^+$ T cells. The experiments were performed twice independently with totally 19 WT mice and 31 VEGF-A Tg mice. Bars represent the mean of each group.

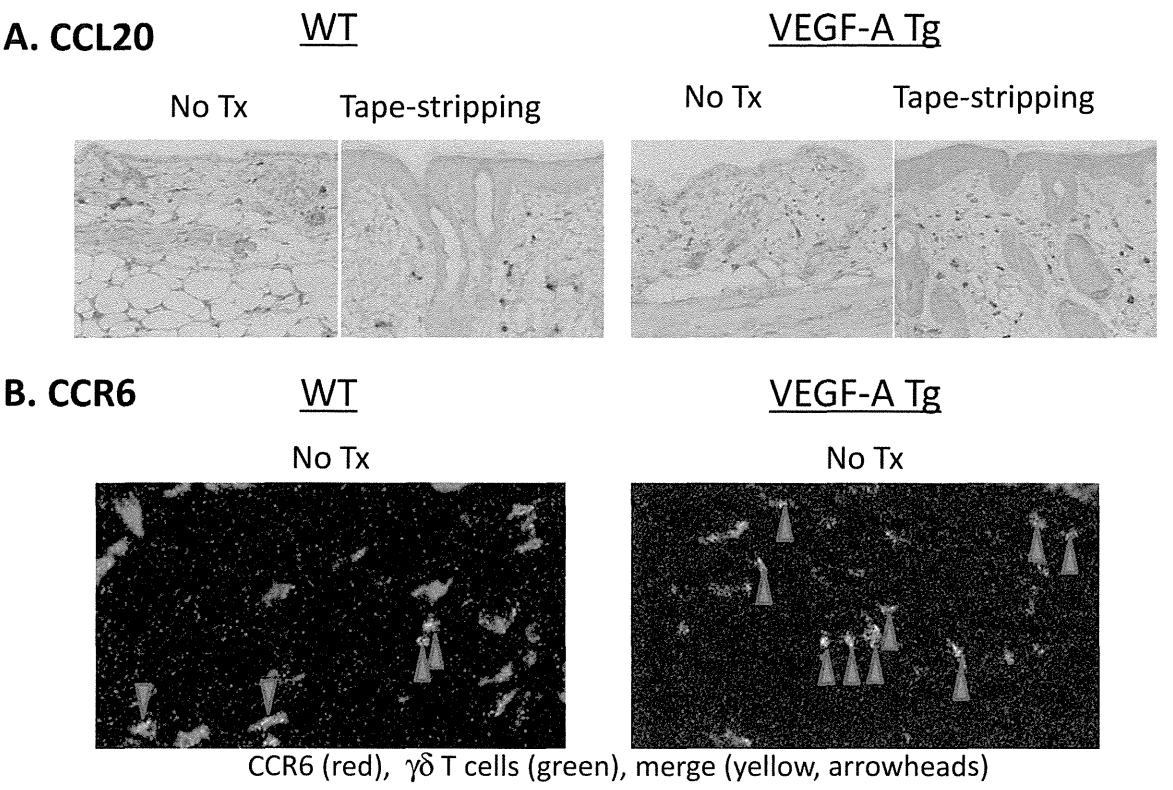


**Fig. 3.** CCL20$^+$ fibroblasts and CCR6$^+$ lymphocytes in abdominal skin of VEGF-A Tg and WT mice. (A) Immunohistochemical staining for CCL20. The number of CCL20$^+$ fibroblasts was increased in the tape-stripped 8-week-old VEGF-A-Tg mice. (B) Double-immunofluorescence staining for CCR6 (red) and γδ TCR (green). Arrowheads indicate merge (yellow) of both CCR6 and γδ TCR. The number of CCR6$^+$ lymphocytes was increased in the tape-stripped 8-week-old VEGF-A-Tg mice. (For interpretation of the references to color in figure legend, the reader is referred to the web version of the article.)

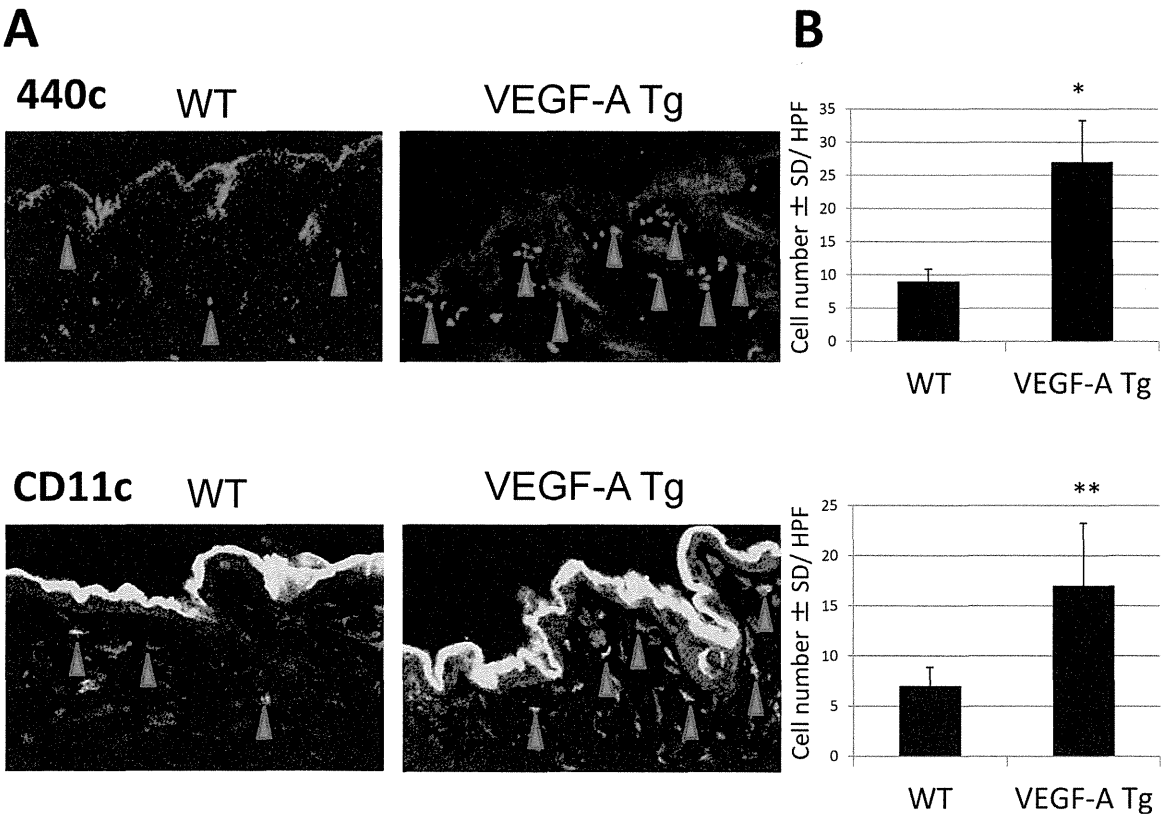


**Fig. 4.** pDCs and CD11c$^+$ DCs infiltrating in abdominal skin of 8-week VEGF-A Tg and WT mice. (A) Immunofluorescence staining of pDCs and CD11c$^+$ DCs. pDCs and CD11c$^+$ DCs were identified as 440c$^+$ cells and CD11c$^+$ cells, respectively. Arrowheads indicate positive cells or clusters of positive cells. (B) The mean numbers ± SD of positive cells/HPF ($n = 3$) are shown. *$P = 0.003$, **$P = 0.08$, compared with WT mice.

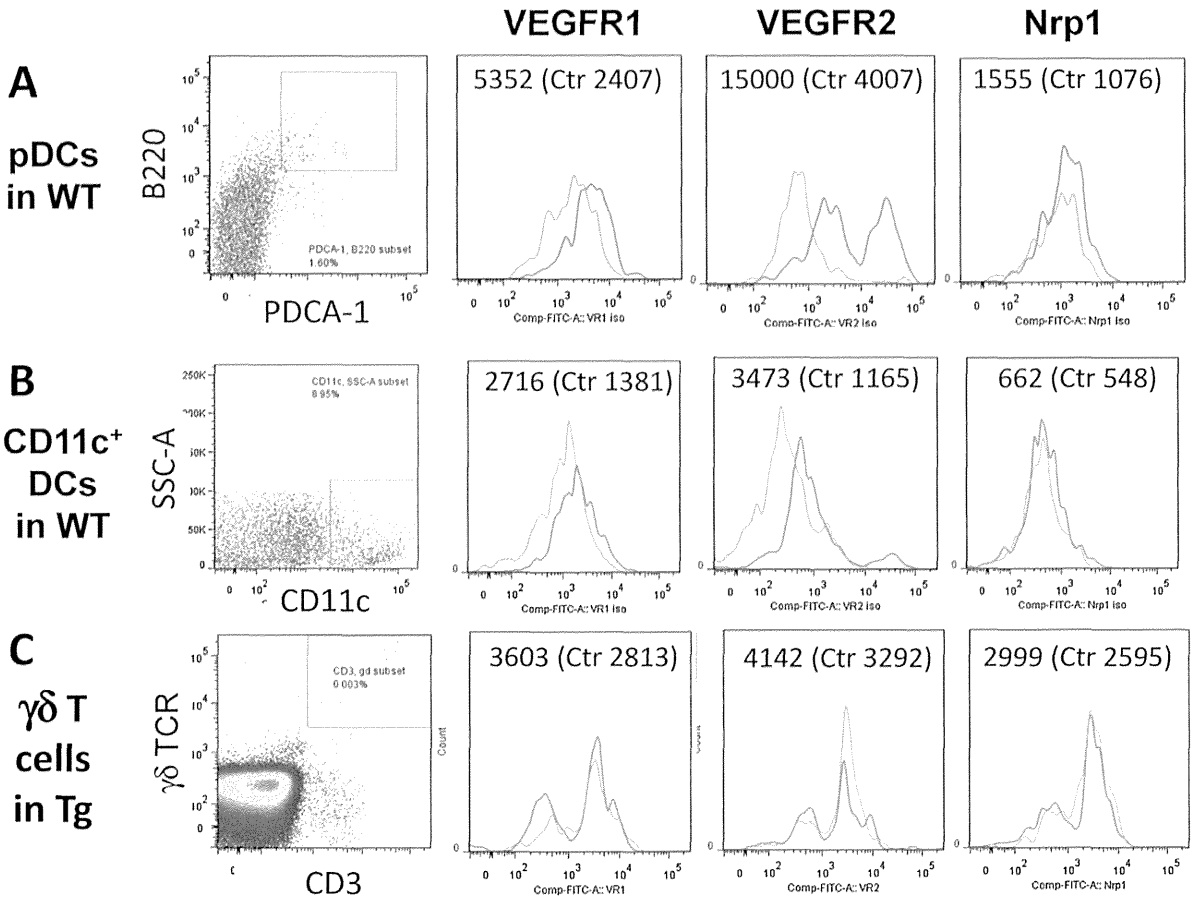


**Fig. 5.** Expressions of VEGFR1, VEGFR2, and Nrp1 in skin-infiltrating pDCs, CD11c$^+$ DCs, and γδ T cells. Skin-infiltrating cells were isolated from ear specimens of WT mice (A, B) or VEGF-A Tg mice (C). (A) For pDCs, cells were stained with anti-PDCA-1 and anti-B220 mAbs and either with anti-VEGFR1, anti-VEGFR2, or anti-Nrp1 mAb. (B) For CD11c$^+$ DCs, cells were stained with anti-CD11c mAb and each mAb to the VEGF receptor. (C) For γδ T cells, cells were stained with anti-CD3 and anti-γδTCR mAbs and with each mAb to the VEGF receptor. pDCs, CD11c$^+$ DCs, and γδ T cells were gated as PDCA-1$^+$B220$^+$ cells, CD11c$^+$ cells, and CD3$^+$γδTCR$^+$ cells, respectively, and the expression levels of VEGFR1, VEGFR2, and Nrp1 were examined (red lines) in parallel with isotype-matched control antibodies (blue lines). The mean fluorescence intensity (MFI) of each receptor expression is shown. Parentheses indicate MFI of control isotype-matched antibodies. (For interpretation of the references to color in figure legend, the reader is referred to the web version of the article.)

Skin-infiltrating cells were isolated from the inflamed ears of VEGF-A Tg mice and analyzed for pDCs by flow cytometry with anti-PDCA-1 and anti-B220 mAbs. pDCs were present in the high forward scatter and side scatter fraction and identified as PDCA-1$^+$ B220$^+$ cells (Fig. 5A). This PDCA-1$^+$ B220$^+$ cell population was CD11c low-positive. The isolated cells (10 mice collectively analyzed) contained a higher percentage of PDCA-1$^+$ B220$^+$ cells in VEGF-A Tg mice ($\sim 3 \times 10^{-3}$%) than in WT mice ($\sim 1 \times 10^{-3}$%). The pDC number in another organ was also examined. In single cell suspensions of spleen cells, the percentages of PDCA-1$^+$ B220$^+$ cells were comparable between VEGF-A Tg ($\sim 134 \times 10^{-3}$%) and WT mice ($\sim 124 \times 10^{-3}$%), indicating preferential infiltration of pDCs in the skin of VEGF-A Tg mice.

Thus, pDCs infiltrate at a high frequency in VEGF-A Tg mice as well as IL-17A$^+$ γδ T cells.

### 3.3. Expressions of VEGFR1, VEGFR2, and Npr1 in skin-infiltrating pDCs and CD11c$^+$ cells, but not γδ T cells

To address the potencies of pDCs, CD11c$^+$ DCs, and IL-17$^+$ γδ T cells to respond to VEGF-A, we examined the expressions of VEGFR1, VEGFR2, and Npr1 on the cells isolated from ears. PDCA-1$^+$ B220$^+$ pDCs in WT mice expressed VEGFR1 and VEGFR2 remarkably and Npr1 weakly (Fig. 5A). CD11c$^+$ DCs also expressed these receptors, but to lesser degrees than pDCs (Fig. 5B). The skin-infiltrating pDCs and CD11c$^+$ DCs from the inflamed ears of VEGF-A Tg mice showed undetectable expression levels of these receptors, suggesting its expression was decreased in activated pDCs. On the other hand, skin-infiltrating γδ T cells did not bear any of these receptors (Fig. 5C).

### 3.4. Expressions of VEGFR1 and VEGFR2 by cultivation of splenic pDCs from WT mice

To test resting pDCs have an ability to express VEGFR1 and VEGFR2 upon stimulation, spleen cells from WT mice were cultured in complete RPMI, and the expression levels of the receptors were monitored in PDCA-1$^+$ B220$^+$ pDCs. Freshly isolated splenic pDCs did not substantially express VEGFR1 or VEGFR2, although Nrp1 expression was high (Fig. 6A). However, when spleen cells were cultured for 48 h, their VEGFR1 expression was markedly and VEGFR2 was moderately elevated, and the Nrp1 expression was reduced but still retained (Fig. 6B). Thus, isolation and cultivation of pDCs augmented the receptor expression. The addition of Toll-like receptor ligand poly(I:C) to the pDC culture in complete RPMI did not further enhance VEGFR1, VEGFR2 or Nrp1 expression (data not shown).

### 3.5. No ability of pDCs to produce cytokines in response to VEGF-A

To evaluate whether VEGF-A functionally stimulates pDCs, we investigated the effects of VEGF-A on cytokine production and

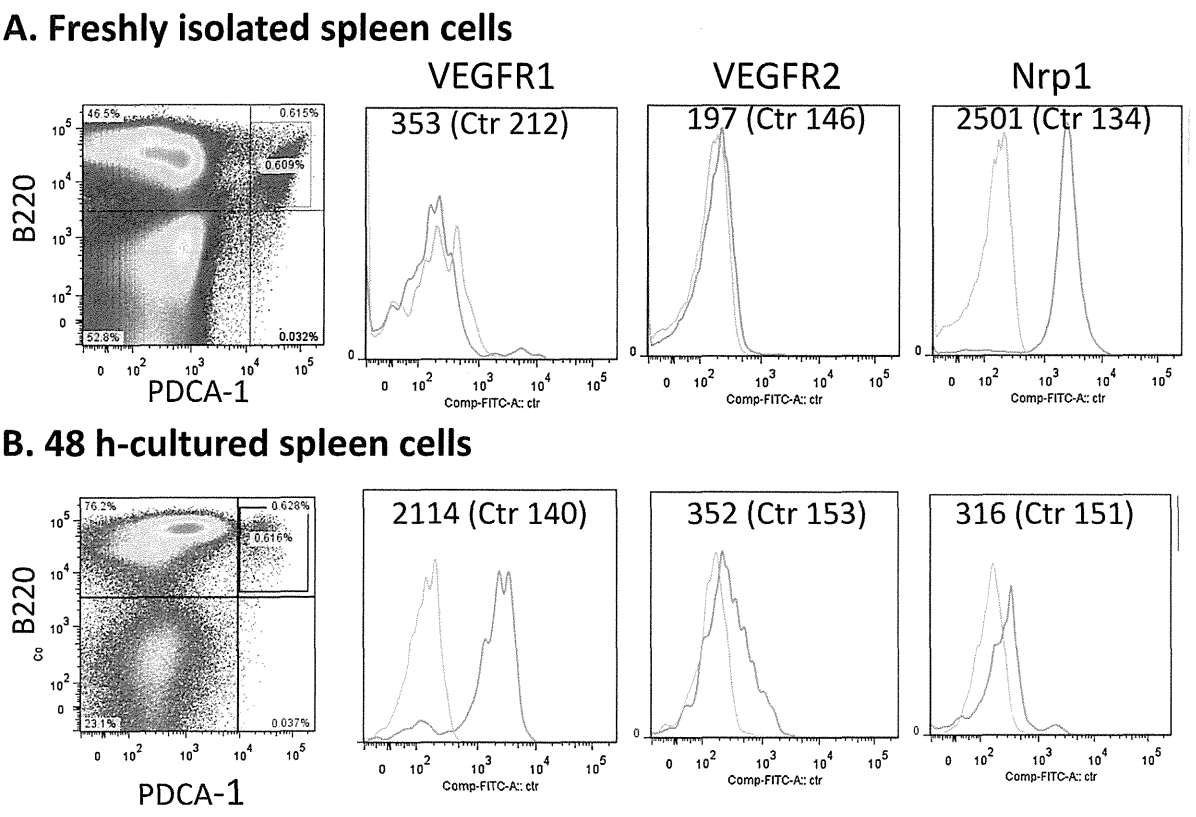


**Fig. 6.** Augmented expressions of VEGFR1 and VEGR2 by cultivation in splenic pDCs. Spleen cell suspensions were prepared from WT mice. Before (A) and after 48-h cultivation (B), they were stained with anti-PDCA-1 and anti-B220 mAbs and either with anti-VEGFR1, anti-VEGFR2, or anti-Nrp1 mAb. PDCA-1$^+$B220$^+$ cells were gated, and the expression levels of VEGFR1, VEGFR2, and Nrp1 were examined (red lines) in parallel with isotype-matched control antibodies (blue lines). The MFI of each receptor expression is shown. Parentheses indicate MFI of control isotype-matched antibody. (For interpretation of the references to color in figure legend, the reader is referred to the web version of the article.)

chemotaxis in both cells. pDC were isolated from WT mouse spleen cells by MACS by negative selection and cultured in the maintenance medium, containing CD40L trimer, GM-CSF, Flt-3 ligand and IL-3, with recombinant VEGF-A for 48 h. The concentrations of IFN-α and TNF-α were measured in the culture supernatants. CpG-ODN, as positive control, stimulated pDCs to produce IFN-α and TNF-α, but VEGF-A was not stimulatory for the production of the two cytokines (Fig. 7).

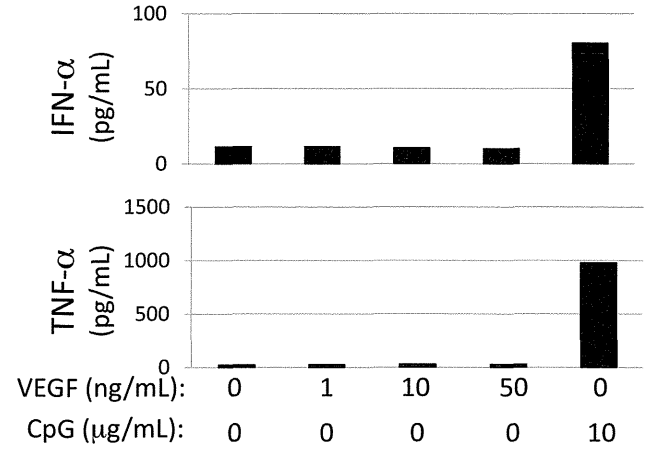


**Fig. 7.** No ability of VEGF-A to stimulate pDCs for cytokine production. pDCs were negatively purified from WT spleen cells. They were cultured for 48 h in complete RPMI-1640 with recombinant VEGF-A or CpG-ODN at the indicated final concentration. The concentrations of IFN-α and TNF-α were measured by ELISA.

### 3.6. Chemotactic activity of pDCs toward VEGF-A

The effects of VEGF-A on the migration of pDCs and CD11c$^+$ DCs were assessed by a chemotaxis assay that allows direct visualization of cell migration. pDCs and CD11c$^+$ DCs were isolated by negative and positive selections, respectively, from WT mouse spleen cells, and time-lapse images of cell migration during chemotaxis were photo-documented by EZ-TAXIScan, plotted, and analyzed by Image J software. The migration traces of pDCs and CD11c$^+$ cells were plotted against time and distance, and velocity was calculated. As shown in representative cells, pDCs migrated toward VEGF-A in a straightforward manner as compared to control (Fig. 8A). The addition of antagonist to VEGFR1, VEGFR2, or Nrp1 yielded random movement, and the addition of both VEGFR1 and VEGFR2 antagonists resulted in velocity reduction. When the mean velocity levels of pDCs toward VEGF-A were calculated, VEGFR1, VEGFR2, Nrp1, and both VEGFR1 and 2 antagonists significantly suppressed the velocity of pDCs toward VEGF-A (Fig. 8B). The chemoattracting ability of VEGF-A was comparable to chemerin, a well-known chemokine for pDCs (Fig. 8B). In contrast, CD11c$^+$ cells showed no chemotaxis toward VEGF-A (Fig. 8C).

## 4. Discussion

Our study showed that γδ T cells, instead of Th17 cells, are the major IL-17-producing T cells in VEGF-A Tg mice. IL-17$^+$ γδ T cells preferentially infiltrated in the skin as compared to the lymph nodes and peripheral blood, suggesting the association of locally released VEGF-A and IL-17$^+$ T cell infiltration. Such an immunological replacement of Th17 cells with γδ T cells has been observed in several murine experimental systems. Dermal γδ T cells in mice

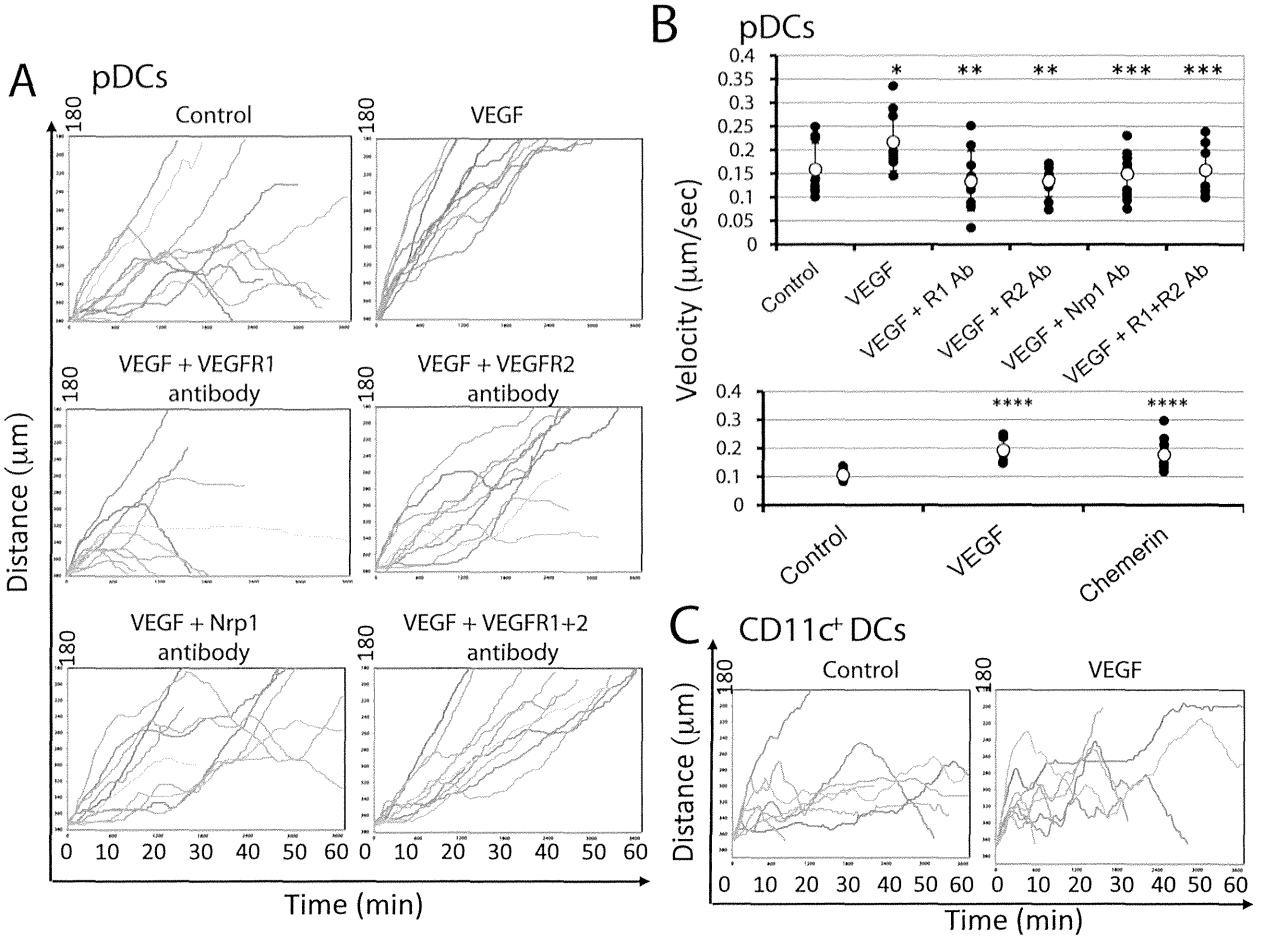


**Fig. 8.** Chemotaxis of pDCs toward VEGF-A. (A) pDC chemotaxis toward VEGF-A. pDCs were purified from WT mouse spleen cells by negative selection. The chemotaxis of pDCs was measured using an EZ-TAXIScan system, an optically accessible horizontal chemotaxis apparatus. Recombinant mouse VEGF 164 at 100 ng/ml was used as chemoattractant. After 60 min, the number of sorted cells that migrated toward VEGF front chamber in a straightforward manner was counted using an Image J. The cells that reached the upper chamber were preferentially considered. For VEGFR1, VEGFR2 and Nrp1 neutralization, pDCs were preincubated with 10 μg/ml of antagonist to VEGFR1, anti-VEGFR2, or anti-Nrp1 for 60 min at 37 °C. (B) Velocity of pDC chemotaxis toward VEGF-A and cxhemerin. From the data shown in (A), the velocity of chemotaxis was calculated in each group. Open circle and vertical bar represent the mean ± SD. $^{*}P < 0.01$, compared with the control group, $^{**}P < 0.01$, $^{***}P < 0.05$, compared with the VEGF group, $^{****}P < 0.01$, compared with the control group. (C) CD11c$^{+}$ DC chemotaxis toward VEGF-A. CD11c$^{+}$ DCs were purified from WT mouse spleen cells by positive selection. The chemotaxis of pDCs was measured as mentioned in (A).

constitutively express the IL-23 receptor and transcriptional factor RORγt, and γδ T cell IL-17 production is independent of αβ T cells [5]. Th17 cells are not the primary source of IL-17A, IL-17F, and IL-22 in mice, and they are produced by a skin-invading population of γδ T cells and RORγt$^{+}$ innate T cells [7]. In human psoriasis, the importance of IL-17-producing γδ T cells is also suggested [5], but its significance remains to be clarified in a comparison with Th17 cells.

More importantly, we found that a high number of pDCs infiltrated in the dermis of VEGF-A Tg mice. The number of DCs and the tissue VEGF amount may be positively or inversely correlated, depending on DC subsets [32]. It is known that activation of dermal pDCs and their IFN-α exacerbate psoriasis in humans [17] and a xenograft model of human psoriasis [18]. In imiquimod-induced psoriasis-like skin inflammation, the numbers of skin-infiltrating pDCs and CD11c$^{+}$ DCs and the expression levels of IL-23, IL-17A, and IL-17F were increased [33]. Toll-like receptor 7 ligation on DCs induced IL-36-mediated crosstalk with keratinocytes and dermal mesenchymal cells that was crucial for control of the pathological IL-23/IL-17/IL-22 axis and disease development [34]. However, the interaction of IFN-α with the Th17-mediated pathogenesis of psoriasis remains poorly understood.

We found that pDCs have receptors for VEGF-A and migrate toward VEGF-A. While skin-infiltrating pDCs expressed VEGFR1 and VEGFR2, splenic pDCs expressed neither VEGFR1 nor VEGFR2. However, when splenic pDCs were cultured for 48 h, they expressed VEGFR1 and VEGFR2, suggesting upregulation of the receptors upon stimulation. It is considered that VEGFR was expressed from an undetectable level to a low but presumably effective level during the chemotaxis assay. Although VEGFR1 was expressed at a higher level than VEGFR2 in cultured splenic pDCs, both VEGFR1 and VEGFR2 antagonists suppressed the pDC chemotaxis toward VEGF-A.

VEGF-A has two tyrosine kinase receptors, VEGFR1 and VEGFR2. VEGFR2 transduces the major signals for angiogenesis with its strong tyrosine kinase activity, and VEGFR1 plays a negative role in embryonic angiogenesis [14]. In macrophage/monocyte-lineage cells, however, VEGFR1 oppositely has a positive role in a tyrosine kinase-dependent manner and promotes inflammation [15]. While macrophages and monocytes produce VEGF [35], they can also respond to VEGF [36]. VEGF is able to elicit a migratory response in monocyte-derived THP-1 cells *via* VEGFR1 [37], and VEGF-A induces chemotaxis of monocytes presumably *via* VEGFR1 [38,39]. These findings are in agreement with our present finding that pDCs

express VEGFR1 and VEGFR2 and have a chemotactic activity toward VEGF-A.

Similarly to pDCs, $CD11c^+$ DCs infiltrated at a higher number in VEGF-A Tg mice than in WT mice. By chemotaxis assay, splenic $CD11c^+$ DCs exhibited no chemotaxis toward VEGF-A. IL-23-producing inflammatory DCs [2] may be contained by the $CD11c^+$ DC fraction and are essential for IL-17 production by Th17 cells or IL-$17^+$ γδ T cells. Our results suggest that VEGF-A contributes to the accumulation of pDCs, but not inflammatory DCs, in the lesional skin. Since IL-$17^+$ γδ T cells did not express VEGFR1 or VEGFR2, VEGF-A is unable to directly stimulate IL-$17^+$ γδ T cells. One possible mechanism underlying the VEGF-A-induced IL-$17^+$ γδ T cell activation is that pDCs interact directly or indirectly with inflammatory DCs to produce IL-23. This issue should be clarified in a future study.

In the pathogenesis of psoriasis, VEGF-A1 is produced from epidermal keratinocytes as a result of stimulation with IL-17 and IL-22 derived from Th17 cells or γδ T cells. In this context, VEGF-A is a downstream factor that induces vascular proliferation in the dermal papillae. However, our study suggests that VEGF-A initiates the psoriatic inflammatory cascade by stimulating pDCs. The tight interaction between VEGF and pDCs may contribute to understanding of the pathogenesis [40], and blocking of the VEGF-induced pDC stimulation is a potential therapeutic target for psoriasis.

## Acknowledgment

This study was supported by Grant-in-Aid from the Ministry of Education, Culture, Sports, Science and Technology in Japan.

## References

[1] Martin DA, Towne JE, Kricorian G, Klekotka P, Gudjonsson JE, Krueger JG, et al. The emerging role of IL-17 in the pathogenesis of psoriasis: preclinical and clinical findings. J Invest Dermatol 2013;133:17–26.
[2] Zaba LC, Krueger JG, Lowes MA. Resident and "inflammatory" dendritic cells in human skin. J Invest Dermatol 2009;129:302–8.
[3] Tokura Y, Mori T, Hino R. Psoriasis and other Th17-mediated skin diseases. J UOEH 2010;32:317–28.
[4] Miossec P, Kolls JK. Targeting IL-17 and TH17 cells in chronic inflammation. Nat Rev Drug Discov 2012;11:763–76.
[5] Cai Y, Shen X, Ding C, Qi C, Li K, Li X. Pivotal role of dermal IL-17-producing γδ T cells in skin inflammation. Immunity 2011;35:596–610.
[6] Gray EE, Ramírez-Valle F, Xu Y, Wu S, Wu Z, Karjalainen KE. Deficiency in IL-17-committed Vγ4(+) γδ T cells in a spontaneous Sox13-mutant CD45.1(+) congenic mouse substrain provides protection from dermatitis. Nat Immunol 2013;14:584–92.
[7] Pantelyushin S, Haak S, Ingold B, Kulig P, Heppner FL, Navarini AA. Rorγt+ innate lymphocytes and γδ T cells initiate psoriasiform plaque formation in mice. J Clin Invest 2012;122:2252–6.
[8] Zheng Y, Danilenko DM, Valdez P, Kasman I, Eastham-Anderson J, Wu J. Nature 2007;445:648–51.
[9] Sano S, Chan KS, DiGiovanni J. Impact of Stat3 activation upon skin biology: a dichotomy of its role between homeostasis and diseases. J Dermatol Sci 2008;50:1–14.
[10] Koga C, Kabashima K, Shiraishi N, Kobayashi M, Tokura Y. Possible pathogenic role of Th17 cells for atopic dermatitis. J Invest Dermatol 2008;128:2625–30.
[11] Canavese M, Altruda F, Ruzicka T, Schauber J. Vascular endothelial growth factor (VEGF) in the pathogenesis of psoriasis – a possible target for novel therapies. J Dermatol Sci 2010;58:171–6.
[12] Simonetti O, Lucarini G, Campanati A, Goteri G, Zizzi A, Marconi B. VEGF, survivin and NOS overexpression in psoriatic skin: critical role of nitric oxide synthases. J Dermatol Sci 2009;54:205–8.
[13] Lohela M, Bry M, Tammela T, Alitalo K. VEGFs and receptors involved in angiogenesis versus lymphangiogenesis. Curr Opin Cell Biol 2009;21:154–65.
[14] Cao Y. Positive and negative modulation of angiogenesis by VEGFR1 ligands. Sci Signal 2009;2:re1.
[15] Shibuya M. Tyrosine kinase receptor Flt/VEGFR family: its characterization related to angiogenesis and cancer. Genes Cancer 2010;1:1119–23.
[16] Boiocchi L, Vener C, Savi F, Bonoldi E, Moro A, Fracchiolla NS. Increased expression of vascular endothelial growth factor receptor 1 correlates with VEGF and microvessel density in Philadelphia chromosome-negative myeloproliferative neoplasms. J Clin Pathol 2011;64:226–31.
[17] Gilliet M, Conrad C, Geiges M, Cozzio A, Thürlimann W, Burg G. Psoriasis triggered by toll-like receptor 7 agonist imiquimod in the presence of dermal plasmacytoid dendritic cell precursors. Arch Dermatol 2004;140:1490–5.
[18] Nestle FO, Conrad C, Tun-Kyi A, Homey B, Gombert M, Boyman O. Plasmacytoid predendritic cells initiate psoriasis through interferon-alpha production. J Exp Med 2005;202:135–43.
[19] Albanesi C, Scarponi C, Pallotta S, Daniele R, Bosisio D, Madonna S. Chemerin expression marks early psoriatic skin lesions and correlates with plasmacytoid dendritic cell recruitment. J Exp Med 2009;206:249–58.
[20] Gregorio J, Meller S, Conrad C, Di Nardo A, Homey B, Lauerma A. Plasmacytoid dendritic cells sense skin injury and promote wound healing through type I interferons. J Exp Med 2010;207:2921–30.
[21] Lande R, Gregorio J, Facchinetti V, Chatterjee B, Wang YH, Homey B. Plasmacytoid dendritic cells sense self-DNA coupled with antimicrobial peptide. Nature 2007;449:564–9.
[22] Detmar M, Brown LF, Schön MP, Elicker BM, Velasco P, Richard L. Increased microvascular density and enhanced leukocyte rolling and adhesion in the skin of VEGF transgenic mice. J Invest Dermatol 1998;111:1–6.
[23] Hirakawa S, Kodama S, Kunstfeld R, Kajiya K, Brown LF, Detmar M. VEGF-A induces tumor and sentinel lymph node lymphangiogenesis and promotes lymphatic metastasis. J Exp Med 2005;201:1089–99.
[24] Xia YP, Li B, Hylton D, Detmar M, Yancopoulos GD, Rudge JS. Transgenic delivery of VEGF to mouse skin leads to an inflammatory condition resembling human psoriasis. Blood 2003;102:161–8.
[25] Hvid H, Teige I, Kvist PH, Svensson L, Kemp K. TPA induction leads to a Th17-like response in transgenic K14/VEGF mice: a novel in vivo screening model of psoriasis. Int Immunol 2008;20:1097–106.
[26] Moll R, Franke WW, Schiller DL, Geiger B, Krepler R. The catalog of human cytokeratins: patterns of expression in normal epithelia, tumors and cultured cells. Cell 1982;31:11–24.
[27] Vassar R, Rosenberg M, Ross S, Tyner A, Fuchs E. Tissue-specific and differentiation-specific expression of a human K14 keratin gene in transgenic mice. Proc Natl Acad Sci USA 1989;86:1563–7.
[28] Colonna M, Trinchieri G, Liu YJ. Plasmacytoid dendritic cells in immunity. Nat Immunol 2004;5:1219–26.
[29] Ito T, Hashizume H, Shimauchi T, Funakoshi A, Ito N, Fukamizu H. CXCL10 produced from hair follicles induces Th1 and Tc1 cell infiltration in the acute phase of alopecia areata followed by sustained Tc1 accumulation in the chronic phase. J Dermatol Sci 2013;69:140–7.
[30] Mohamedali KA, Poblenz AT, Sikes CR, Navone NM, Thorpe PE, Darnay BG. Inhibition of prostate tumor growth and bone remodeling by the vascular targeting agent VEGF121/rGel. Cancer Res 2006;66:10919–28.
[31] Chakraborty G, Kumar S, Mishra R, Patil TV, Kundu GC. Semaphorin 3A suppresses tumor growth and metastasis in mice melanoma model. PLOS ONE 2012;7:e33633.
[32] Kikuchi K, Kusama K, Sano M, Nakanishi Y, Ishige T, Ohni S. Vascular endothelial growth factor and dendritic cells in human squamous cell carcinoma of the oral cavity. Anticancer Res 2006;26:1833–48.
[33] van der Fits L, Mourits S, Voerman JS, Kant M, Boon L, Laman JD. Imiquimod-induced psoriasis-like skin inflammation in mice is mediated via the IL-23/IL-17 axis. J Immunol 2009;182:5836–45.
[34] Tortola L, Rosenwald E, Abel B, Blumberg H, Schäfer M, Coyle AJ. Psoriasiform dermatitis is driven by IL-36-mediated DC-keratinocyte crosstalk. J Clin Invest 2012;122:3965–76.
[35] Haneda Y, Hasegawa S, Hirano R, Hashimoto K, Ohsaki A, Ichiyama T. Leukotriene D4 enhances tumor necrosis factor-α-induced vascular endothelial growth factor production in human monocytes/macrophages. Cytokine 2011;55:24–8.
[36] Block MS, Nevala WK, Leontovich AA, Markovic SN. Differential response of human and mouse dendritic cells to VEGF determines interspecies discrepancies in tumor-mediated TH1/TH2 polarity shift. Clin Cancer Res 2011;17:1776–83.
[37] Zhu C, Xiong Z, Chen X, Lu Z, Zhou G, Wang D. Soluble vascular endothelial growth factor (VEGF) receptor-1 inhibits migration of human monocytic THP-1 cells in response to VEGF. Inflamm Res 2011;60:769–74.
[38] Czepluch FS, Olieslagers S, van Hulten R, Vöö SA, Waltenberger J. VEGF-A-induced chemotaxis of CD16+ monocytes is decreased secondary to lower VEGFR-1 expression. Atherosclerosis 2011;215:331–8.
[39] Muramatsu M, Yamamoto S, Osawa T, Shibuya M. Vascular endothelial growth factor receptor-1 signaling promotes mobilization of macrophage lineage cells from bone marrow and stimulates solid tumor growth. Cancer Res 2010;70:8211–21.
[40] Schonthaler HB, Huggenberger R, Wculek SK, Detmar M, Wagner EF. Systemic anti-VEGF treatment strongly reduces skin inflammation in a mouse model of psoriasis. Proc Natl Acad Sci USA 2009;106:21264–69.

Journal of Dermatological Science 75 (2014) 43–48

Contents lists available at ScienceDirect

Journal of Dermatological Science

journal homepage: www.jdsjournal.com

# Induction of cytotoxic T cells as a novel independent survival factor in malignant melanoma with percutaneous peptide immunization

Toshiharu Fujiyama [a,*], Isao Oze [b], Hiroaki Yagi [a], Hideo Hashizume [a], Keitaro Matsuo [c], Ryosuke Hino [d], Riei Kamo [e], Shuhei Imayama [f], Satoshi Hirakawa [a], Taisuke Ito [a], Masahiro Takigawa [a], Yoshiki Tokura [a]

[a] Department of Dermatology, Hamamatsu University School of Medicine, Japan
[b] Division of Epidemiology and Prevention, Aichi Cancer Center Research Institute, Japan
[c] Department of Preventive Medicine, Kyusyu University, Japan
[d] Department of Dermatology, University of Occupational and Environmental Health, Japan
[e] Department of Dermatology, Osaka City University Graduate School of Medicine, Japan
[f] Imayama Shuhei Clinic & Lab, Japan

ARTICLE INFO

*Article history:*
Received 5 February 2014
Received in revised form 3 April 2014
Accepted 5 April 2014

*Keywords:*
Percutaneous peptide immunization
Melanoma
Cytotoxic T lymphocytes

ABSTRACT

*Background:* Malignant melanoma (MM) often shows multiple chemo-resistance, leading to poor prognosis of the patients. Therapeutic anti-cancer vaccination may be a feasible way to prolong the survival of patients. We have demonstrated that application of antigenic peptides *via* the tape-stripped, horny layer-removed skin, known as percutaneous peptide immunization (PPI), induces tumor cell-specific cytotoxic T lymphocytes (CTLs) in rodents and humans.
*Objective:* To evaluate clinical significance of PPI in advanced MM patients.
*Methods:* We performed PPI in 59 patients undergoing advanced MM with Melan-A, tyrosinase, MAGE-2, MAGE-3 and gp-100 peptides based on HLA typing in individuals. The induction of CTLs was assessed by the tetramer or pentamer flow cytometry in 35 patients. Patients showing positive CTL responses to all antigens were defined as complete responder ($n = 18$), and those showing negative responses to at least one applied antigen were classified as incomplete responder ($n = 17$). The primary endpoint of the study was overall survival (OS). For statistical analysis, log-rank test, univariate and multivariate Cox proportional hazard model were used.
*Results:* OS of the complete responders was longer than that of the incomplete responders (median survival time: 55.8 vs 20.3 months, log rank $P = 0.089$). A hazard ratio for the complete responders relative to the incomplete responders was 0.23 (95% confidence interval: 0.06–0.93, $P = 0.039$) in a multivariate Cox proportional hazard model.
*Conclusion:* The induction of CTLs was a novel independent survival factor, and the induction of peptide-specific CTLs by PPI contributes to the prolonged survival and represents an impact on therapeutic approaches in MM.
Unique trial number: UMIN000005706.


## 1. Introduction

Malignant melanoma (MM) represents an aggressive skin neoplasm and shows rapid tumor progression and metastasis, leading to a reduced patient survival. Metastatic cutaneous MM is often resistant to conventional therapies, such as chemotherapy, radiation, and surgical resection. On the other hand, MM has a highly immunogenic property, as represented by spontaneous regression occasionally seen in primary tumors [1]. Therefore,

*Abbreviations:* APC, antigen-presenting cells; CTLs, cytotoxic T lymphocytes; DC, dendritic cells; MM, malignant melanoma; OS, overall survival; PBMCs, peripheral blood mononuclear cells.

* Corresponding author at: Department of Dermatology, Hamamatsu University School of Medicine, Handayama 1-20-1, Higashi-ku, Hamamatsu 431-3192, Japan. Tel.: +81 53 435 2303; fax: +81 53 435 2368.
*E-mail address:* fujiyama@hama-med.ac.jp (T. Fujiyama).

http://dx.doi.org/10.1016/j.jdermsci.2014.04.005
0923-1811/

immunotherapy was initially applied to MM, and there have been a considerable number of clinical studies on the immunological treatment modalities for MM [2–4]. Effective presentation of the defined tumor antigens is one of the key factors to develop a durable immunotherapy for advanced MM. Furthermore, the antigen recognition and subsequent antigen-mediated cytotoxicity by T cells infiltrating in tumor microenvironment are essential for efficient promotion of tumor elimination. Clinically, it remains to be elucidated whether the occurrence of antigen-specific T cell responses can be an indicator for prolongation of the patients' survival.

Depletion of T cell-mediated immune responses results in a rapid tumor growth in experimental animal models [5]. Cytotoxic $CD8^+$ T lymphocytes (CTLs) recognize tumor-associated antigens [6–8]. Adoptive transfer of tumor-specific CTLs is capable of eradicating certain types of tumors [9,10], suggesting that CTLs are crucial for tumor-specific adaptive immunity. CTLs attack tumor cells expressing tumor-associated antigenic peptides with major histocompatibility complex (MHC) class I on the cell surface. When $CD8^+$ T cells recognize the tumor-specific antigen, they produce interferon-γ (IFN-γ) and mediate cytostasis and cell death. Furthermore, $CD8^+$ T cells promote cell cycle inhibition, apoptosis and angiostasis, and induce the tumoricidial activity of macrophages in tumor microenvironment [11,12].

Antigen-presenting dendritic cells (DCs) play an important role in mediating antigen-specific T-cell responses [9]. Immunotherapies have been improved with the knowledge that T cell antitumor activity can be enhanced with antibodies against immunoregulatory molecules (checkpoint blockade). Current immunotherapy strategies include monoclonal antibodies against tumor cells or immunoregulatory molecules, cell-based therapies such as adoptive transfer of *ex vivo*-activated T cells and natural killer cells, and cancer vaccines. It is an issue how the current understanding of DC and T cell biology might enable the development of next-generation cancer vaccine therapies [13]. Emerging evidence has shown that DC-based vaccination may be potent, while the corresponding method requires a particular technique. Thus, a simple and efficacious procedure is desired for the efficient antigen vaccination and presentation.

We have previously established the simple method by attaching peptide vaccines on the barrier-disrupted skin so that MM-specific CTLs can be induced in a mouse model and a small number of patients [14,15]. This study shows the advantage of novel percutaneous peptide immunization (PPI) for advanced melanoma patients. Based on this finding, we subjected the simple technique to 59 advanced MM patients in multi-institutional joint research. We identified, for the first time, that the induction of CTLs reveals an independent prognostic factor for MM patients.

## 2. Materials and methods

### 2.1. Eligibility and study design

Patients were eligible those who were histologically confirmed as MM, aged 20 years or older, compatible with HLA-A0201 or HLA-A2402. Patients were ineligible with the history of previous chemotherapy, vaccination within 4 weeks, or macroscopic metastatic lesions in the liver or brain. The other ineligible factors included present pregnancy, immunosuppressant administration, and coexistence of eczematous lesions, hepatitis or collagen diseases. All patients provided a written informed consent. The present study was approved by the ethics committee of Hamamatsu University School of Medicine. The study design was an open labeled, single arm, prospective and interventional trial.

### 2.2. Synthetic peptides

Four custom-synthesized peptides including tyrosinase (AFLPWHRLF), MAGE-2 (EYLQLVFGI), MAGE-3 (IMPKAGLLI) and gp-100 (VWKTWGQYW; all from Peptide Institute, Inc., Osaka, Japan) were used as HLA-A2402-restricted epitopes. Modified Melan-A immunodominant cells (ELAGIGLTV; Peptide Institute) were used as HLA-A0201-restricted epitopes [16]. Respective purity was >95% as confirmed by high-pressure liquid chromatography.

### 2.3. Epidermal barrier disruption

To remove *stratum corneum*, 5 cm × 5 cm square plastic plates were evenly painted with 100 mg/plate of cyanoacrylate (Aron alpha A Sankyo, Tokyo, Japan) or PPT3 tape (LINTEC, Tokyo, Japan), which were attached to the skin for 3 min and removed gently. This procedure was repeated three times at a single spot.

### 2.4. Percutaneous peptide immunization (PPI)

Respective solution of immunization peptides was made prior to topical application. HLA-A0201 subjects received 3 mg of Melan-A peptide in 3 ml of 5% DMSO in phosphate buffered saline (PBS). A cocktail of 3 mg each of tyrosinase, MAGE-2, MAGE-3, and gp-100 peptide in 3 ml of 5% DMSO in PBS was used for HLA-A2402 subjects. In patients who had both HLA-A0201 and HLA-A2402, we used 3 mg of all peptides in 3 ml of 5% DMSO in PBS. Right after the removal of *stratum corneum* (Fig. 1A, top, middle), respective peptide solution was soaked up by the gauze pads (each 5 cm × 5 cm), which were then applied to each of six barrier-disrupted areas (total area 150 $cm^2$) and immediately covered with a dressing film (Fig. 1A, bottom). The pads were removed 24 h later. We avoided the area close to the lymph nodes surgically resected. PPI was repeated ten times at monthly intervals by placing the patches at different areas of the skin. Stable and responding patients were followed up, and when the frequencies of all CTLs became lower than 50% of their maximum points, the patients were eligible for the second cycle of vaccination.

### 2.5. Measurement of immune responses by flow cytometry

Peripheral blood was collected from the patients just before and 3–6 months after the PPI. Peripheral blood mononuclear cells (PBMCs) were purified by standard Ficoll density centrifugation and subjected to flow cytometric analysis. Blood samples were run on a FACS Calibur flow cytometer (BD Bioscience, San Jose, CA) using Cell Quest Software. Phycoerythrin (PE)-labeled MHC pentamers specific for tyrosinase, MAGE-2 and MAGE-3, were custom-synthesized by ProImmune Limited (Littlemore, UK). PE-labeled tetramer for Melan-A was purchased from Beckman Coulter (Villepinte, France). PE-labeled tetramers specific for HIV gag (SLYNTVATL) for HLA-A0201 and tetramers specific for Cytomegalovirus pp65 (QYDPVAALF) or tetramers specific for Epstain–Barr virus BMLF-1 (DYNFVKQLF) for HLA-A2402 were used as controls. PBMCs were stained with PE-labeled HLA-A0201 tetramers or PE-labeled HLA-A2402 pentamers and T-Select Antibodies Gating Kit according to the manufacture's direction (Medical & Biological Laboratories Co.) including FITC-labeled anti-CD8, PC5-labeled anti-CD4, anti-CD19, and anti-CD13 monoclonal antibodies (mAbs). We analyzed $1.0 \times 10^5$ PBMCs for CTLs specific to each antigen. Because no HLA-A2402 pentamer or tetramer for gp-100 was available, patients with HLA-A2402 were evaluated with for only tyrosinase, MAGE-2 and MAGE-3-specific CTLs. The frequencies of antigen-specific CTLs from HLA-matched healthy donors were used as control ($n = 6$ for both types of HLA).

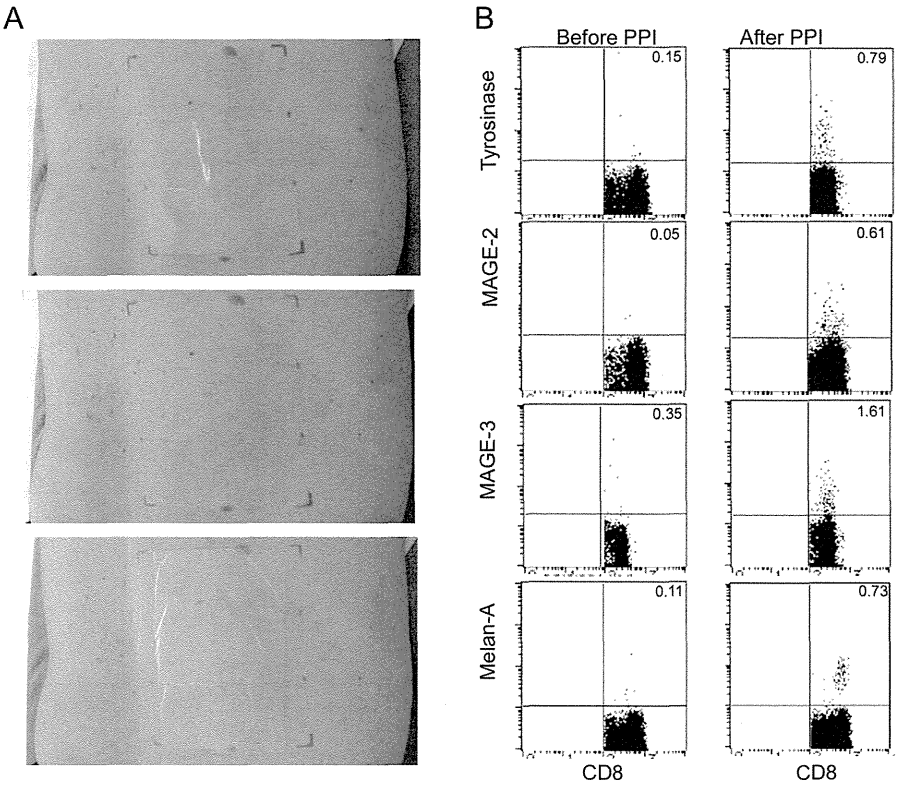


**Fig. 1.** Demonstration of PPI and representative data of flowcytometric analysis of tetramer/pentamer-positive CD8 cells. (A) To remove the *stratum corneum*, PPT3 tape is attached to the skin for 3 min (top) and removed gently (middle). This procedure was repeated three times. The treated skin becomes slightly reddish. Then, the peptide-containing pad is topically applied and covered with a film (bottom). The exposure of the peptides to the skin is performed for 24 h. (B) $CD8^+$ cells are on the *x*-axis and tetramer/pentamer-positive cells are on the *y*-axis.

### 2.6. CTL response evaluation

When the frequency of the antigen-specific CTLs was equal or greater than mean + 2SD of the control, we considered the value as positive. When it was lower than mean + 2SD of the control, it was considered negative. Patients showing positive responses to all applied antigens were defined as complete responder, and those showing negative responses to at least one applied antigen were classified as incomplete responder. Therefore, the incomplete responder also included the complete non-responder.

### 2.7. Clinical response evaluation

Tumor evaluation included physical examination and axial computed tomography (CT) scans before treatment. Stable and responding patients were evaluated every 6 months by physical examination, blood tests and CT scan. Overall response was evaluated by modification of Response Evaluation Criteria in Solid Tumors (RECIST 1.1).

### 2.8. Statistical analysis

The analysis aimed at determining whether high responders to PPI have a better prognosis than do the low or non-responders. The primary endpoint of the study was overall survival (OS), which was defined as the interval between the date of PPI initiation and the date of death or last follow-up. The survival curve was calculated by Kaplan–Meier product limit method. The association between OS and prognostic factors were assessed by HR and 95% CI used multivariate Cox proportional hazard model using Landmark method [17]. As the study did not employ randomization because of the properties of the study, we defined multivariate analysis adjusted for established prognostic factors as a primary analysis. Potential confounding factors considered in the multivariate analysis were age as a continuous variable, sex (male or female), primary site (limbs, mucosa, or others), LDH (<400 IU/L or ≥400 IU/L), PS (0, 1, or 2–4), history of chemotherapy (never or ever), and disease stage (I–III or IV). For reference, univariate analysis was done by the log-rank test and univariate Cox proportional hazard models. Statistical analyses were performed using STATA version 10 (Stata Corporation, College Station, TX). The frequencies of specific CTLs were compared by Wilcoxon *T* test. We defined a priori *P*-value less than 0.05 in a primary analysis as threshold to indicate significant impact of induction of CTLs by PPI. For other analyses, we conventionally applied *P*-value less than 0.05 as statistically significant.

## 3. Results

In April 2003 to March 2011, 59 patients with advanced MM were subjected to PPI by using the *stratum corneum*-removal tape-stripping technique (Fig. 1A). No hematologic abnormality was observed after PPI. The most frequent adverse events were generalized progressive vitiligo (12 out of 59 patients) after several months of immunization. Four patients had irritant dermatitis at the treated sites.

CTLs were evaluated in 35 patients before and after PPI, and 24 patients were excluded in the following analysis, because CTLs were not examined either pre- or post-PPI or both. Among the 35 patients, 27 and 15 patients were positive for HLA-A2402 and A0201, respectively. Seven patients were positive for both HLA types. As represented by a patient responding well to PPI (Fig. 1B), the dot-plot flow cytometry revealed the frequencies of $CD8^+$ CTLs specific to tyrosinase, MAGE-2, MAGE-3, and Melan-A were all increased after 3 to 6-time PPI treatments as compared to the pre-PPI values.

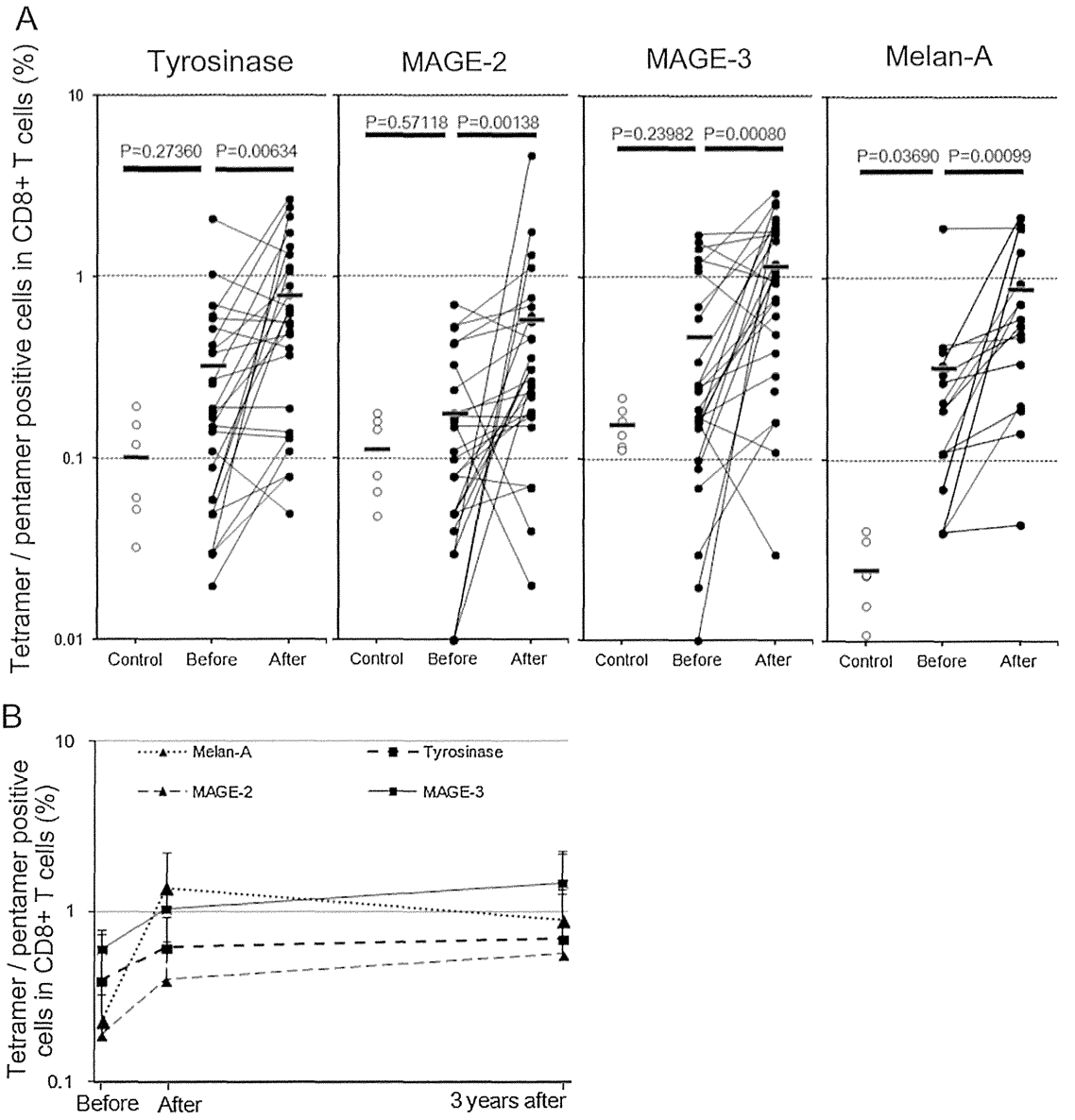


**Fig. 2.** Percentage of each tetramer/pentamer-positive cells in CD8$^+$ T cells. (A) The frequencies of CD8$^+$ CTLs specific to tyrosinase, MAGE-2, MAGE-3, and Melan-A were monitored before and after 3 to 6-time PPI treatments. The control represents the data from healthy subjects. (B) Three-year follow up of the frequencies of the applied antigen-specific CLTs ($n$ = 3 for Melan-A, $n$ = 6 for tyrosinase, MAGE-2 and MAGE-3).

Even before PPI treatment, the frequencies of peptide-specific CTLs in MM patients were largely higher than those of the healthy control subjects. The pre-therapy CTL frequencies to Melan-A were significantly higher, and those to the other three antigens tended to be higher than the controls (Fig. 2A). More importantly, the CTL frequencies further increased significantly after PPI. The $P$-values for tyrosinase-, MAGE-2-, MAGE-3- and Melan-A-specific CTLs were 0.006, 0.001, 0.001 and 0.001, respectively (Wilcoxon $t$-test). We examined the degree of patients' responsiveness to PPI by monitoring the CTL frequencies. Among the patients with HLA A2402, 19 of 27, 19 of 27 and 23 of 27 patients developed positive responses to tyrosinase, MAGE-2 and MAGE-3, respectively (Fig. 2A). We monitored the frequencies of CTL for 3 years in several complete responders. The frequencies of the antigen-specific CTL remained or slightly increased in the patients who survived and showed positive responses to tyrosinase, MAGE-2, and MAGE-3 (Fig. 2B), presumable by the repeated course of immunization. In addition, among the patients with HLA A0201, 12 of 15 patients developed positive responses to Melan-A. Eighteen patients showed positive responses to all applied peptide antigens, and we defined them as complete responders. The rest of the patients ($n$ = 17) were negative for at least one applied antigen, and we defined them as incomplete responders. Among the incomplete responders, 2 patients were negative to all applied antigens. There was no significant difference in the patients' characteristics between the complete and incomplete responders (Table 1).

The overall survival time in the complete and incomplete responders were investigated by Kaplan–Meier method (Fig. 3). At a median follow-up time of 16.2 months, the complete responder group had a longer survival than the incomplete responder group (MST; 55.8 vs 20.3 months, $P$ = 0.089). Univariate and multivariate analyses were performed to examine the relationship between OS and CTL induction (Table 2). The multivariate analysis was adjusted for age, sex, primary site, LDH, PS, history of chemotherapy, and disease stage. The complete responder group had a significantly higher survival than did the incomplete responder group (HR = 0.23, 95% CI: 0.06–0.93, $P$ = 0.039). This association was consistently observed when we exclude primary site from the

**Table 1**
Patient characteristics.

| | CTL induction | | P |
|---|---|---|---|
| | Complete responder | Incomplete-responder | |
| Age (mean, SD) | | | 0.687 |
| | 54.9 ± 16.9 | 57.3 ± 18.1 | |
| Sex | | | 0.631 |
| Male | 12 | 10 | |
| Female | 6 | 7 | |
| Primary site | | | 0.128 |
| Limb | 9 | 5 | |
| Mucosa | 0 | 3 | |
| Other | 9 | 9 | |
| LDH | | | 0.714 |
| <400 IU/L | 15 | 14 | |
| ≥400 IU/L | 1 | 2 | |
| PS | | | 0.803 |
| 0, 1 | 16 | 14 | |
| ≥2 | 1 | 2 | |
| History of chemotherapy | | | 0.113 |
| Never | 2 | 6 | |
| Ever | 16 | 10 | |
| Disease stage | | | 0.369 |
| I–III | 3 | 5 | |
| IV | 15 | 12 | |

model (data not shown). Univariate analysis showed consistent association between OS and CTL response after PPI. Since we used a cocktail of the peptides, we were unable to directly compare the efficacy of each peptide. Among the incomplete responders, however, we observed no significant correlation between the overall survival and the antigen incapable of inducing positive responses. Moreover, there was no significant difference in the overall survival between HLA-A0201 and A2402 (log-rank $P = 0.213$), suggesting that there was no priority in the efficacy of A0201 or A2402-related peptides.

## 4. Discussion

It was reported that the objective response (PR + CR) in the DC vaccination therapies with peptides was 7.8% [18]. In the present study, at least 3-month period was required for the induction of CTLs. Since 50 of 59 patients showed PD, we were able to monitor the frequencies of CTLs after PPI in only 35 patients. Nevertheless, we showed that the superior survival of advanced MM patients significantly correlated with the complete induction of peptide-specific CTLs by PPI. Multivariate analyses further revealed that the complete responder is an independent survival factor in the MM patients who received PPI. Thus, the vaccination has a clinical impact on therapeutic approaches in metastatic MM. Even before the PPI treatment, the frequencies of specific CTLs in the blood were higher than the controls, and they further increased after the treatment, suggesting the contribution of CTLs to the therapeutic

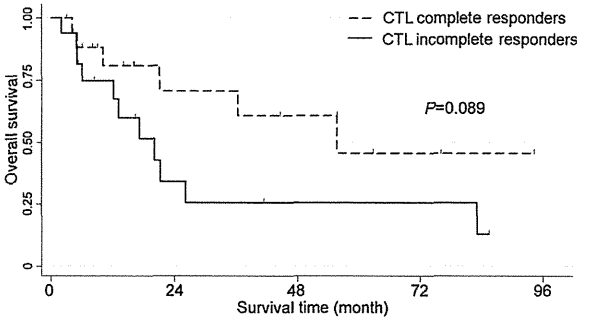


**Fig. 3.** Overall survival time in association with CTL induction. Patients showing positive responses to all four antigens were defined as complete responder, and those showing negative responses to at least one applied antigen were classified as incomplete responder. The complete responders show a superior survival as compared with the incomplete responders by Kaplan–Meier method.

effect. We have previously shown that peptide-specific CTLs are successfully induced by PPI and infiltrate in the tumor lesions, and can reduce the tumor size [14]. In agreement with our finding, it was reported that the presence of tumor-infiltrating lymphocytes in the primary sites or in the metastatic foci of lymph nodes is an independent prognostic factor for cutaneous MM [19,20]. Since Melan A and tyrosinase are expressed not only in melanoma cells but also by normal melanocytes, autoimmune reactions possibly occur against normal melanocytes, as the development of ocular and systemic autoimmunity following the immunotherapy has been documented. All of our patients were screened for uveitis before and after the PPI and none showed positive findings. The common adverse events were systemic progressive vitiligo, seen in 12 patients, but no life threatening side effect was observed.

On the other hand, recent studies have suggested that MM is resistant to the $CD8^+$ T cell-based vaccination therapy. A number of mechanisms have been put forward to explain the resistance [21]. The tumor induces peripheral tolerance of tumor-specific $CD8^+$ T cells by their clonal deletion [22] or peripheral anergy [23,24], or induction of regulatory T cells [25]. The tumor cell *per se* develops immune evasion mechanisms to prevent recognition and killing by CTLs [26]. More recently, promotion of PD-1/PD-L1 engagement [27] and suppression of Th17-derived cytokines [28] have been shown to down-modulate the CTL-mediated melanoma immunity. The MM-specific $CD8^+$ T cell was detected in peripheral blood of 68% of advanced stage MM patients, but the induction of these cells was not accompanied by clinically significant antitumor effect [29]. For efficacious control of the disease, antigen-specific CTLs should be functionally active, capable of homing to the tumor sites, and resistant to the tumor microenvironment.

We used cutaneous DCs as APCs. Recently, the classical paradigm for LCs has been revised. LCs migrate to draining lymph nodes and initiate T cell priming. However, LCs may not be indispensable for contact hypersensitivity, but even serve as a

**Table 2**
The association between CTL induction and overall survival.

| | | Univariate analysis | | | Multivariate analysis | | |
|---|---|---|---|---|---|---|---|
| | | HR | 95% CI | P | HR | 95% CI | P |
| CTL induction | Incomplete vs complete | 0.43 | (0.16–1.17) | 0.098 | 0.23 | (0.06–0.93) | 0.039 |
| Age | | 0.97 | (0.94–1.00) | 0.076 | 0.97 | (0.92–1.01) | 0.141 |
| Sex | Male vs female | 1.01 | (0.37–2.76) | 0.979 | 0.83 | (0.18–3.90) | 0.815 |
| Primary site | Limb | 1.00 | Ref. | | 1.00 | Ref. | |
| | Mucosa | 1.02 | (0.20–5.11) | 0.985 | 0.37 | (0.06–2.47) | 0.306 |
| | Other | 1.61 | (0.57–4.59) | 0.373 | 0.46 | (0.05–3.86) | 0.472 |
| LDH | <400 vs ≥400 IU/L | 3.14 | (0.68–14.50) | 0.143 | 1.05 | (0.10–10.96) | 0.969 |
| PS | 0,1 vs 2–4 | 19.91 | (1.11–358.25) | 0.042 | 25.31 | (0.85–756.82) | 0.062 |
| Chemotherapy | Never vs ever | 0.86 | (0.27–2.72) | 0.803 | 0.53 | (0.09–3.04) | 0.476 |
| Disease stage | I–III vs IV | 1.50 | (0.49–4.66) | 0.479 | 3.32 | (0.62–17.78) | 0.162 |

regulator for the sensitivity in mice [30,31]. In the tumor immunity, however, the depletion of LCs at the time of skin immunization dramatically reduced the tumor-protective effect [32], suggesting the importance of LCs for percutaneous immunization. LCs can clearly fulfill an immunogenic role during vaccination against cancer *in vivo* [33]. Although the role of LCs in the induction of skin immune responses remains to be constitutively demonstrated, immunization strategies of antigen application to the skin have been proven to be feasible and to elicit systemic immunity [34,35]. Accordingly, several challenges for the induction of anti-tumor immune responses using LCs or cutaneous DCs have been reported [9,14,32,36].

To our knowledge, this is the first report demonstrating the effective induction of the tumor specific CTLs in MM patients who received PPI treatment. Our study suggests that PPI is simple and safe and relatively effective treatment for MM, and thus, it can be one of the therapeutic options. To improve the response rate and overall survival, selection of antigenic peptides, addition of helper epitope peptides, and usage of adjuvants should be considered in future.

## Acknowledgment

This study was supported by Grants-in-Aid for Scientific Research from the Ministry of Health, Labour, and Welfare in Japan.

## References

[1] Morton DL, Wanek L, Nizze JA, Elashoff RM, Wong JH. Improved long-term survival after lymphadenectomy of melanoma metastatic to regional nodes. Analysis of prognostic factors in 1134 patients from the John Wayne Cancer Clinic. Ann Surg 1991;214. 491–9, discussion 499–501.
[2] Fang L, Lonsdorf AS, Hwang ST. Immunotherapy for advanced melanoma. J Invest Dermatol 2008;128:2596–605.
[3] Tuting T. T cell immunotherapy for melanoma from bedside to bench to barn and back: how conceptual advances in experimental mouse models can be translated into clinical benefit for patients. Pigment Cell Melanoma Res 2013;26:441–56.
[4] Topalian SL, Weiner GJ, Pardoll DM. Cancer immunotherapy comes of age. J Clin Oncol 2011;29:4828–36.
[5] Koebel CM, Vermi W, Swann JB, Zerafa N, Rodig SJ, Old LJ, et al. Adaptive immunity maintains occult cancer in an equilibrium state. Nature 2007;450:903–7.
[6] Ikeda H, Ohta N, Furukawa K, Miyazaki H, Wang L, Kuribayashi K, et al. Mutated mitogen-activated protein kinase: a tumor rejection antigen of mouse sarcoma. Proc Natl Acad Sci U S A 1997;94:6375–9.
[7] van der Bruggen P, Traversari C, Chomez P, Lurquin C, De Plaen E, Van den Eynde B, et al. A gene encoding an antigen recognized by cytolytic T lymphocytes on a human melanoma. Science 1991;254:1643–7.
[8] Wolfel T, Hauer M, Schneider J, Serrano M, Wolfel C, Klehmann-Hieb E, et al. A p16INK4a-insensitive CDK4 mutant targeted by cytolytic T lymphocytes in a human melanoma. Science 1995;269:1281–4.
[9] Grabbe S, Beissert S, Schwarz T, Granstein RD. Dendritic cells as initiators of tumor immune responses: a possible strategy for tumor immunotherapy? Immunol Today 1995;16:117–21.
[10] Banchereau J, Steinman RM. Dendritic cells and the control of immunity. Nature 1998;392:245–52.
[11] Smyth MJ, Dunn GP, Schreiber RD. Cancer immunosurveillance and immunoediting: the roles of immunity in suppressing tumor development and shaping tumor immunogenicity. Adv Immunol 2006;90:1–50.
[12] Dunn GP, Old LJ, Schreiber RD. The three Es of cancer immunoediting. Annu Rev Immunol 2004;22:329–60.
[13] Palucka K, Banchereau J. Dendritic-cell-based therapeutic cancer vaccines. Immunity 2013;39:38–48.
[14] Yagi H, Hashizume H, Horibe T, Yoshinari Y, Hata M, Ohshima A, et al. Induction of therapeutically relevant cytotoxic T lymphocytes in humans by percutaneous peptide immunization. Cancer Res 2006;66:10136–44.
[15] Seo N, Tokura Y, Nishijima T, Hashizume H, Furukawa F, Takigawa M. Percutaneous peptide immunization via corneum barrier-disrupted murine skin for experimental tumor immunoprophylaxis. Proc Natl Acad Sci U S A 2000;97:371–6.
[16] Sliz P, Michielin O, Cerottini JC, Luescher I, Romero P, Karplus M, et al. Crystal structures of two closely related but antigenically distinct HLA-A2/melanocyte-melanoma tumor-antigen peptide complexes. J Immunol 2001;167:3276–84.
[17] Anderson JR, Cain KC, Gelber RD. Analysis of survival by tumor response. J Clin Oncol 1983;1:710–9.
[18] Nakai N, Hartmann G, Kishimoto S, Katoh N. Dendritic cell vaccination in human melanoma: relationships between clinical effects and vaccine parameters. Pigment Cell Melanoma Res 2010;23:607–19.
[19] Clemente CG, Mihm Jr MC, Bufalino R, Zurrida S, Collini P, Cascinelli N. Prognostic value of tumor infiltrating lymphocytes in the vertical growth phase of primary cutaneous melanoma. Cancer 1996;77:1303–10.
[20] Mihm Jr MC, Clemente CG, Cascinelli N. Tumor infiltrating lymphocytes in lymph node melanoma metastases: a histopathologic prognostic indicator and an expression of local immune response. Lab Invest 1996;74:43–7.
[21] Huang Y, Shah S, Qiao L. Tumor resistance to CD8+ T cell-based therapeutic vaccination. Arch Immunol Ther Exp (Warsz) 2007;55:205–17.
[22] Aichele P, Brduscha-Riem K, Zinkernagel RM, Hengartner H, Pircher H. T cell priming versus T cell tolerance induced by synthetic peptides. J Exp Med 1995;182:261–6.
[23] Van Parijs L, Abbas AK. Homeostasis and self-tolerance in the immune system: turning lymphocytes off. Science 1998;280:243–8.
[24] Shevach EM. CD4+ CD25+ suppressor T cells: more questions than answers. Nat Rev Immunol 2002;2:389–400.
[25] Seo N, Hayakawa S, Takigawa M, Tokura Y. Interleukin-10 expressed at early tumour sites induces subsequent generation of CD4(+) T-regulatory cells and systemic collapse of antitumour immunity. Immunology 2001;103:449–57.
[26] Lee HM, Timme TL, Thompson TC. Resistance to lysis by cytotoxic T cells: a dominant effect in metastatic mouse prostate cancer cells. Cancer Res 2000;60:1927–33.
[27] Hino R, Kabashima K, Kato Y, Yagi H, Nakamura M, Honjo T, et al. Tumor cell expression of programmed cell death-1 ligand 1 is a prognostic factor for malignant melanoma. Cancer 2010;116:1757–66.
[28] Hayata K, Iwahashi M, Ojima T, Katsuda M, Iida T, Nakamori M, et al. Inhibition of IL-17A in tumor microenvironment augments cytotoxicity of tumor-infiltrating lymphocytes in tumor-bearing mice. PLoS One 2013;8:e53131.
[29] van Oijen M, Bins A, Elias S, Sein J, Weder P, de Gast G, et al. On the role of melanoma-specific CD8+ T-cell immunity in disease progression of advanced-stage melanoma patients. Clin Cancer Res 2004;10:4754–60.
[30] Kaplan DH, Jenison MC, Saeland S, Shlomchik WD, Shlomchik MJ. Epidermal langerhans cell-deficient mice develop enhanced contact hypersensitivity. Immunity 2005;23:611–20.
[31] Kissenpfennig A, Henri S, Dubois B, Laplace-Builhe C, Perrin P, Romani N, et al. Dynamics and function of Langerhans cells in vivo: dermal dendritic cells colonize lymph node areas distinct from slower migrating Langerhans cells. Immunity 2005;22:643–54.
[32] Stoitzner P, Green LK, Jung JY, Price KM, Tripp CH, Malissen B, et al. Tumor immunotherapy by epicutaneous immunization requires langerhans cells. J Immunol 2008;180:1991–8.
[33] Romani N, Clausen BE, Stoitzner P. Langerhans cells and more: langerin-expressing dendritic cell subsets in the skin. Immunol Rev 2010;234:120–41.
[34] Warger T, Schild H, Rechtsteiner G. Initiation of adaptive immune responses by transcutaneous immunization. Immunol Lett 2007;109:13–20.
[35] Partidos CD, Beignon AS, Semetey V, Briand JP, Muller S. The bare skin and the nose as non-invasive routes for administering peptide vaccines. Vaccine 2001;19:2708–15.
[36] Eisenberg G, Machlenkin A, Frankenburg S, Mansura A, Pitcovski J, Yefenof E, et al. Transcutaneous immunization with hydrophilic recombinant gp100 protein induces antigen-specific cellular immune response. Cell Immunol 2010;266:98–103.

OPEN ACCESS Freely available online

PLOS | ONE

# Lymphangiogenesis and Angiogenesis in Abdominal Aortic Aneurysm

**Masaki Sano[1,7], Takeshi Sasaki[2], Satoshi Hirakawa[3], Junichi Sakabe[3], Mikako Ogawa[4], Satoshi Baba[5], Nobuhiro Zaima[6,8], Hiroki Tanaka[1,7], Kazunori Inuzuka[1,7], Naoto Yamamoto[1,7], Mitsutoshi Setou[6], Kohji Sato[2], Hiroyuki Konno[7], Naoki Unno[1,7]***

**1** Division of Vascular Surgery, Applied Medical Photonics Laboratory, Medical Photonics Research Center, Hamamatsu City, Shizuoka, Japan, **2** Department of Anatomy and Neuroscience, Applied Medical Photonics Laboratory, Medical Photonics Research Center, Hamamatsu City, Shizuoka, Japan, **3** Department of Dermatology, Applied Medical Photonics Laboratory, Medical Photonics Research Center, Hamamatsu City, Shizuoka, Japan, **4** Department of Molecular Imaging, Applied Medical Photonics Laboratory, Medical Photonics Research Center, Hamamatsu City, Shizuoka, Japan, **5** Department of Diagnostic Pathology, Hamamatsu University School of Medicine, Hamamatsu, Shizuoka, Japan, **6** Department of Cell Biology and Anatomy, Hamamatsu University School of Medicine, Hamamatsu, Shizuoka, Japan, **7** Second Department of Surgery, Hamamatsu University School of Medicine, Hamamatsu, Shizuoka, Japan, **8** Department of Applied Biological Chemistry, Kinki University, Osaka, Japan

## Abstract

The pathogenesis of abdominal aortic aneurysm (AAA) is characterized to be inflammation-associated degeneration of vascular wall. Neovascularization is regularly found in human AAA and considered to play critical roles in the development and rupture of AAA. However, little is known about lymphangiogenesis in AAA. The purpose of this study was to demonstrate both angiogenesis and lymphangiogenesis in AAA. Abdominal aortic tissue was harvested either from autopsy (control group) and during open-repair surgery for AAA (AAA group). Adventitial lymphatic vasa vasorum was observed in both groups, but seemed to be no significant morphological changes in AAA. Immunohistochemical studies identified infiltration of lymphatic vessel endothelial hyaluronan receptor (LYVE) −1, vascular endothelial growth factor (VEGF)-C, and matrix metalloproteinase (MMP)-9-positive macrophages and podoplanin and Prox-1-positive microvessels in the intima/media in AAA wall, where hypoxia-inducible factors (HIF)-1α was expressed. VEGF-C and MMP-9 were not expressed in macrophages infiltrating in the adventitia. Intraoperative indocyanine green fluorescence lymphography revealed lymph stasis in intima/medial in AAA. Fluorescence microscopy of the collected samples also confirmed the accumulation of lymph in the intima/media but not in adventitia. These results demonstrate that infiltration of macrophages in intima/media is associated with lymphangiogenesis and angiogenesis in AAA. Lymph-drainage appeared to be insufficient in the AAA wall.

**Citation:** Sano M, Sasaki T, Hirakawa S, Sakabe J, Ogawa M, et al. (2014) Lymphangiogenesis and Angiogenesis in Abdominal Aortic Aneurysm. PLoS ONE 9(3): e89830. doi:10.1371/journal.pone.0089830

**Editor:** Utpal Sen, University of Louisville, United States of America

**Received** September 13, 2013; **Accepted** January 23, 2014; **Published** March 20, 2014



**Funding:** This work was supported partly by a Grant-in-Aid for Scientific Research (C) (22591400) (to N.U.) from Japan Society for the Promotion of Science (JSPS) for purchasing reagents or analysis tools. No additional external funding was received for this study. The funder had no role in study design, data collection and analysis, decision to publish, or preparation of the manuscript.

**Competing Interests:** The authors have declared that no competing interests exist.

* E-mail: unno@hama-med.ac.jp

## Introduction

Abdominal aortic aneurysm (AAA) is a common disease among elderly people. AAA affects 5–10% of men over 65 years and is the tenth leading cause of death in men over the age of 55 years in the United States [1]. When surgical treatment is inapplicable, AAA progress to rupture with a high mortality (30–50%). An effective nonsurgical therapy is currently not available, because the precise mechanisms of AAA pathogenesis is yet to be identified. The degeneration of vascular wall has been considered as one of the main causes of AAA onset and rupture. Previous studies have demonstrated infiltration of inflammatory cells, such as macrophages, T cells, neutrophils and dendric cells, into the aortic wall [2,3]. These inflammatory cells are considered to contribute to the pathogenesis of AAA through the secretion of inflammatory mediators, including cytokines, chemokines, and MMPs [4]. In AAA, an intraluminal thrombus prevents luminal perfusion of oxygen, allowing only the adventitial vasa vasorum (VV) to deliver oxygen and nutroents to the aortic wall. We have recently demonstrated the arteriosclerotic degeneration of VV and tissue ischemia in AAA wall [5]. These inflammatory and hypoxic environment are potential stimuli for angiogenesis as previously reported [6]. Angiogenesis is thought to contribute to destructive processes within the AAA wall and plays a key role in aortic aneurysm development and rupture [7]. In various chronic inflammatory situations such as asthma, atopic dermatitis, rheumatoid arthritis, and inflammatory bowel diseases, both angiogenesis and lymphangiogenesis occur simultaneously to glow neovessels to remodel vascular structure [8–10]. However, little is known about lymphangiogenesis in AAA. Here, we investigated the presence of lymphanagiogenesis and major drivers of angiogenesis and lymphangiogenesis such as VEGF-A and VEGF-C in AAA wall using AAA samples which were obtained during open repair of AAA surgery.

## Materials and Methods

### Sample collection

All procedures used in this study and the use of samples obtained at autopsy were approved by the Ethics Committee of Clinical Research of the Hamamatsu University School of Medicine. We enrolled 20 consecutive patients who underwent elective open surgery to repair infrarenal AAAs at the Division of Vascular Surgery, Hamamatsu University School of Medicine, between May 2010 and August 2013 and obtained written informed consent for use of the sample from each patient. The aortic tissue was dissected during surgery. Longitudinal tissue strips were resected from the infrarenal aortic neck to the bifurcation.

Twenty aorta obtained at autopsy were used as controls. Written informed consent was also obtained from the donor-family for use of the sample with approval of the Ethics Committee of Clinical Research of the Hamamatsu University School of Medicine. The mid-portion of the abdominal aorta between the renal artery and the bifurcation was resected and collected from routine autopsies between October 2011 and February 2013 in the Department of Pathology, Hamamatsu University Hospital. Autopsy specimens from patients with collagen disease, aortic aneurysm/dissection, or under the age of 18 years were excluded.

Atherosclerotic risk factors (hypertension, hypercholesterolemia, hypertriglyceridemia, diabetes, and smoking) were investigated in AAA patients and autopsy cases. The definition of each item was as follows: hypertension (medication for hypertension or a systolic blood pressure $\geq$140 mmHg and/or a diastolic blood pressure $\geq$90 mmHg), hypercholesterolemia (medication for hypercholesterolemia or total cholesterol concentration in the serum of $\geq$220 mg/dL), hypertriglyceridemia (medication for hypertriglyceridemia or total triglyceride in the serum of $\geq$150 mg/dL), diabetes (present or past medication for diabetes), smoking (present or past smoking history).

Resected aortic tissues were immersed in 10% neutral buffered formalin for at least 24 h for histological and immunohistochemical staining. These samples were embedded in paraffin; 4 μm sections were cut and mounted onto MAS-coated slides (Matsunami, Osaka, Japan). The aortic tissue was frozen in liquid nitrogen, and fresh frozen tissue was stored at −80°C for quantitative real-time polymerase chain reaction analysis and near-infrared fluorescence microscopy, and immunohistochemical staining.

### Histological and immunohistochemical staining

Paraffin sections were deparaffinized in xylene, rehydrated in solutions of decreasing alcohol concentration, and stained routinely with elastica van Gieson (EVG) staining. Immunohistochemical staining for podoplanin, CD31, vascular endothelial growth factor (VEGF)-A, VEGF-C, vascular endothelial growth factor receptor (VEGFR)-1, VEGFR-2, VEGFR-3, Ki-67, human hypoxia-inducible factor 1 alpha (HIF-1α), macrophages, CD3, CD19, and myeloperoxidase (MPO) were performed. The following primary antibodies were used: mouse monoclonal antibody clone D2-40 (1:200, DakoCytomation, Glostrup, Denmark) to identify podoplanin in lymphatic endothelial cells, rabbit polyclonal antibody against a synthetic peptide corresponding to the C-terminus of CD31 (1:100, AnaSpec, CA, USA) to identify vascular endothelial cells, mouse monoclonal antibody against human VEGF-A (1:50, Abcam, Tokyo, Japan), rabbit polyclonal antibody against human VEGF-C (1:50, Abcam, Tokyo, Japan), rabbit monoclonal antibody against human VEGFR-1 (1:100, Epitomics, CA, USA), rabbit polyclonal antibody against human VEGFR-2 (1:200, Abcam, Tokyo, Japan), rabbit polyclonal antibody against human VEGFR-3 (1:400, Santa Cruz Biotechnology, CA, USA), rabbit polyclonal antibody against Ki-67 (1:500, Novus Biologicals, CO, USA), mouse monoclonal antibody against human HIF-1α (1:100, Novus Biologicals, CO, USA), mouse monoclonal antibody against human macrophages (1:100, AbD Serotec, Oxford, UK), mouse monoclonal antibody against human CD3 (1:100, LifeSpan Biosciences, Seatle, WA), mouse monoclonal against human CD19 (1:50, Santa Cruz Biotechnology, CA, USA), and mouse monoclonal antibody against human myeloperoxidase (MPO) (1:50, Santa Cruz Biotechnology, CA, USA). The sections were deparaffinized, dehydrated, and boiled in a pressure cooker in 0.01 M citric acid buffer (pH 6.0) for 20 min. The sections were washed with phosphate-buffered saline and incubated with 3% $H_2O_2$ in absolute methanol for 5 min to inhibit any endogenous peroxidase activity. Sections were preincubated with 3% normal goat serum for 20 min to minimize nonspecific binding to the primary antibody, and incubated with the primary antibodies at 4°C overnight in a moist chamber. The sections were washed with phosphate-buffered saline and then incubated with the appropriate secondary antibody for 30 min at room temperature. Staining was visualized with Vector DAB (3,3′-diaminobenzidine, Vector Laboratories, CA, USA), and sections were then counterstained with hematoxylin.

Immunohistochemical staining was also performed on frozen sections. Aortic tissues were embedded in Tissue-Tek OCT compound (Miles Inc., Elkhart, IN, USA), frozen in liquid nitrogen, and stored at −80°C. Frozen sections of 5-μm thickness were prepared using a cryostat (Microm HM560 cryostat, Thermo Scientific, Bremen, Germany), and mounted onto MAS-coated slides (Matsunami, Osaka, Japan). The sections were fixed for 10 min with 4% paraformaldehyde phosphate buffer solution (Wako, Osaka, Japan) and washed with phosphate-buffered saline. The sections were incubated with 3% $H_2O_2$ in absolute methanol for 5 min to inhibit any endogenous peroxidase activity, preincubated with 3% normal goat serum for 20 min to minimize nonspecific binding to the primary antibody, and incubated with the primary antibodies at 4°C overnight in a moist chamber. The sections were washed with phosphate-buffered saline and then incubated with the appropriate secondary antibody for 30 min at room temperature. Staining was visualized with Vector DAB (3,3′-diaminobenzidine, Vector Laboratories, CA, USA), and sections were then counterstained with hematoxylin.

### Double immunofluorescence staining

Colocalization studies were performed with double immunofluorescence staining methods. The following primary antibodies were used: mouse monoclonal antibody against podoplanin (1:200, DakoCytomation, Glostrup, Denmark), rabbit polyclonal antibody against Prox-1 (1:2000, Millipore, MA, USA), rabbit polyclonal antibody against the N-terminus of human alpha smooth muscle isoform of actin (1:25, Thermo Scientific Japan, Tokyo, Japan), mouse monoclonal antibody against human HIF-1α (1:100, Novus Biologicals, CO, USA), rabbit monoclonal antibody against human CD11b (1:250, Millipore, MA, USA), mouse monoclonal antibody against human macrophages (1:100, AbD Serotec, Oxford, UK), rabbit polyclonal antibody against human LYVE-1 (1:100, Relia Tech, Braunschweig, Germany), rabbit polyclonal antibody against human VEGF-C (1:50, Abcam, Tokyo, Japan), rabbit polyclonal antibody against human matrix metalloproteinase (MMP)-9 (1:100, Abnova, Taipei, Taiwan), mouse monoclonal antibody against human CD3 (1:100, LifeSpan Biosciences, Seattle, WA), mouse monoclonal antibody against human CD19 (1:50, Santa Cruz Biotechnology, CA, USA), mouse monoclonal antibody against human myeloperoxidase (MPO) (1:50, Santa

Cruz Biotechnology, CA, USA), rabbit polyclonal antibody against transforming growth factor beta-1 (TGF-β1) (1:50, Abbiotec, CA, USA), rabbit polyclonal antibody against human interleukin-4 (IL-4) (1:50, Biozol, Munich, Germany), rabbit polyclonal antibody against human interleukin-8 (IL-8) (1:50, Abnova, Taipei, Taiwan), rabbit polyclonal antibody against human macrophage inflammatory protein-1α (MIP-1α) (1:50, Spring bioscience, CA, USA), rabbit polyclonal antibody against human interferon-γ (IFN-γ) (1:50, Santa Cruz Biotechnology, CA, USA), and rabbit polyclonal antibody against human monocyte chemotactic protein-1 (MCP-1) (1:50, Abnova, Taipei, Taiwan). The sections were deparaffinized, dehydrated, and boiled in a pressure cooker in 0.01 M citric acid buffer (pH 6.0) for 20 min. The sections were washed with phosphate-buffered saline and incubated with 3% $H_2O_2$ in absolute methanol for 5 min to inhibit any endogenous peroxidase activity, preincubated with 3% normal chicken serum for 20 min to minimize nonspecific binding to the primary antibody, and incubated with the primary antibodies at 4°C overnight in a moist chamber. Immunoreactivity was visualized using Alexa Fluor 488-conjugated anti-mouse IgG, Alexa Fluor 594-conjugated anti-mouse IgG, Alexa Fluor 488-conjugated anti-rabbit IgG, and Alexa Fluor 594-conjugated anti-rabbit IgG (Life Technologies, CA, USA). All Alexa Fluor-conjugated secondary antibodies were diluted 200-fold for use. The slides were mounted in glycerol-based Vectashield medium containing the nucleus stain DAPI (Vector Laboratories, CA, USA).

### Morphometric analysis

Immunohistochemical staining for podoplanin was performed to detect lymphatic vessels. Podoplanin was expressed in aortic intima and some podoplanin-positive cells formed microvessels. Lymphatic microvessel (LMV) density and lymphatic microvessel area in the intima were counted per microscopic field [11,12]. The 10 areas with the highest podoplanin-positive areas within the intima ('hot spots') were selected at low magnification (×40) [13]. Lymphatic microvessel density was then determined by counting all immunostained microvessels per ×200 microscopic field using a computerized image analysis system (Lumina Vision version 3.0, Mitani Corp. Tokyo, Japan). The percentage of lymphatic microvessel area, consisting of the podoplanin-positive cells plus the vessel lumen, per ×200 microscopic field (corresponding to an examination area of 0.136 $mm^2$) was also measured using the computerized image analysis system [11,12,14,15].

### Near-infrared fluorescence lymphography and microscopy of aneurysmal walls

In AAA patients, near-infrared fluorescence lymphography of the AAA wall was performed intraoperatively. The method was performed as previously described [16].Before open surgical aneurysm repair, 0.3 mL of indocyanine green (ICG; Daiichi Pharmaceutical, Tokyo, Japan; 5 mg/mL saline solution) was subcutaneously injected into the dorsum of each foot. Laparotomy was performed, and the AAA wall was observed with Photodynamic Eye near-infrared camera system (PDE-neo, Hamamatsu Photonics, Hamamatsu, Japan) 2 h after ICG injection. Portions of AAA walls were resected and frozen in liquid nitrogen, and 10 μm frozen sections were cut. The following near-infrared fluorescence microscopy procedure was performed with the use of an upright epifluorescence microscope (Eclipse 80i, Nikon Instruments Inc., NY, USA) with a microscopic near-infrared camera system (Photometrics Evolve 512, Nippon Roper, Tokyo, Japan) to evaluate lymphatic fluid in AAA walls. Fluorescence images were obtained with the ICG fluorescence filter (ICG-B-000, excitation wavelength 769±20.5 nm, emission wavelength 832±18.5 nm, Opto-Line, Tokyo, Japan), antifade reagent (ProLong Gold antifade reagent with DAPI, Life Technologies Japan, Tokyo, Japan), and exposure time 200 μseconds. Pseudo-color images were generated using a computerized image analysis system (Lumina Vision version 3.0, Mitani Corp. Tokyo, Japan). Serial frozen sections of 5 μm thickness were prepared using a cryostat. EVG staining and immunohistochemical staining for podoplanin and macrophages were also performed.

### Quantitative real-time polymerase chain reaction analysis for VEGF and VEGFR gene products

Aortic walls were frozen in liquid nitrogen and stored at −80°C. Fresh frozen aortic tissues were placed into TRIzol reagent (Life Technologies, CA, USA), and homogenized with a mechanical rotor for 1 min. Total mRNA was isolated and purified using the PureLink RNA Mini Kit (Life technologies, CA, USA) according to the protocol for using TRIzol with the PureLink RNA Mini Kit as recommended by the manufacturer. The total RNA concentration of individual sample was determined by spectrophotometer analysis (Nano-drop Technologies, DE, USA) at 260 nm. Reverse transcription was performed using TaqMan Reverse Transcription Reagents (Life Technologies Japan, Tokyo, Japan), and cDNA was prepared from 1000 μg total RNA. Real-time quantitative polymerase chain reaction (PCR) of each sample was carried out with TaqMan Gene Expression Assays and an ABI Prism 7700 Sequence Detection System (Applied Biosystems, CA, USA), based on methods described previously [17]. The Taqman assays used were VEGF-A (Hs00900055_m1), VEGF-C (Hs00153458_m1), c-fos induced growth factor (VEGF-D, Hs01128657_m1), fms-related tyrosine kinase 1 (VEGFR-1, Hs01052961_m1), kinase insert domain receptor (a type III receptor tyrosine kinase, VEGFR-2, Hs00911700_m1), and fms-related tyrosine kinase 4 (VEGF-3, Hs01047677_m1) from Applied Biosystems. Data were analyzed by comparative Ct method [18]. For each sample, the Ct value was divided by that of the housekeeping gene, actin beta (Hs01060665_g1), to generate the standardized Ct value.

### Statistical analysis

Lymphatic microvessel density and the percentage of lymphatic microvessel area in the intima are expressed as means ± SE. Differences between normal aorta and AAA were analyzed by Student's t-test.

Categorical variables were reported as frequencies with percentages, and compared between control and AAA groups using Fisher's exact test to obtain P-values. All continuous data were expressed as mean value ± SE, and compared between control and AAA groups using Student's t-test. Statistical significance of differences was defined as a P-value of $<0.05$. All statistical analyses were performed using SPSS 17.0 for Windows (SPSS Inc., IL, USA).

## Results

### Patient characteristics

Twenty AAA cases (16 male, 4 female; age 68.7±1.5 y) and 20 autopsy specimens (11 male, 9 female; age 66.5±3.0 y) were included in this study (Table 1). Male sex was more common among AAA patients compared with controls, but this difference was not statistically significant. Neither age nor BMI significantly differed between the AAA and control groups. The diameter of the abdominal aorta was larger in the AAA group than in the control group. The prevalence of hypertension, hypercholesterolemia, and

**Table 1.** Baseline characteristics of the AAA group and control group.

| Category | Aneurysm (n = 20) | Control (n = 20) | *P* value |
|---|---|---|---|
| Sex (M/F) | 16/4 | 11/9 | 0.176 |
| Age | 68.7±1.5 | 66.5±3.0 | 0.528 |
| BMI | 21.8±0.7 | 21.2±0.7 | 0.619 |
| Diameter of abdominal aorta | 49.8±2.7 | 18.0±0.7 | <0.001 |
| Hypertension (+/−) | 15 (75%)/5 (25%) | 11 (55%)/9 (45%) | 0.320 |
| Hypercholesterolemia (+/−) | 9 (45%)/11 (55%) | 5 (25%)/15 (75%) | 0.320 |
| Hypertriglyceridemia (+/−) | 7 (35%)/13 (65%) | 8 (40%)/12 (60%) | 1.000 |
| Diabetes (+/−) | 3 (15%)/17 (85%) | 4 (20%)/16 (80%) | 1.000 |
| Smoking (+/−) | 15 (75%)/5 (25%) | 11 (55%)/9 (45%) | 0.320 |

The definition of each item: hypertension (medication for hypertension or a systolic blood pressure ≥140 mmHg and/or a diastolic blood pressure ≥90 mmHg), hypercholesterolemia (medication for hypercholesterolemia or total cholesterol concentration in the serum of ≥220 mg/dL), hypertriglyceridemia (medication for hypertriglyceridemia or total triglyceride in the serum of ≥150 mg/dL), diabetes (present or past medication for diabetes), smoking (present or past smoking history).
doi:10.1371/journal.pone.0089830.t001

cigarette smoking were more common in AAA group compared with the control group, but these differences were not statistically significant. The prevalence of hypertriglyceridemia, and diabetes mellitus were not statistically different between the AAA and control groups.

## Lymphatic microvessels in the intima of abdominal aortic aneurysm

Elastica van Gieson (EVG) staining of AAA walls revealed intimal thickening and degradation of the wavy structure of elastin fibers in media compared with normal aorta (Fig. 1A, B). Immunohistochemical staining indicated that podoplanin was rarely expressed in the intima of normal aorta and frequently expressed in that of AAA (Fig. 1C, D). Additionally, some podoplanin-positive cells in the intima of AAA formed vessels (Fig. 1E).

Double immunofluorescence staining revealed that the nuclei of vessel-forming, podoplanin-positive cells in the intima of AAA expressed Prox-1 (Fig. 1F–I). Colocalization of podoplanin and the alpha smooth muscle isoform of actin was not detected in the intima of AAA (Fig. 1J–M).

Immunohistochemical staining indicated that podoplanin was expressed in the adventitia of normal aorta and AAA. Immunohistochemical staining of adventitial lymphatic vessels seemed indicate no morphological changes between the walls of normal aorta and AAA (Fig. 1N, O).

Lymphatic microvessel density in the intima was 243.0±59.3 (vessels/10 fields) in the control group and 938.4±85.7 (vessels/10 fields) in AAA group ($P<0.001$; Fig. 1P). The percentage of lymphatic microvessel area was 1.3±0.4% in the control group and 4.5±0.4% in the AAA group ($P<0.001$; Fig. 1Q).

## Lymphangiogenesis and angiogenesis in AAA

EVG staining of AAA walls showed degradation of the wavy structure of elastin fibers in the media, where numerous microvessels were distributed from intima to media (Fig. 2A, B). Podoplanin-positive microvessels and CD31-positive microvessels were present (Fig. 2C, D). Furthermore, expressions of vascular endothelial growth factor receptor (VEGFR)-1, VEGFR-2, and VEGFR-3 increased in the microvessels (Fig. 2E–G). VEGF-A or VEGF-C- positive cells were also seen within and around the microvessels (Fig. 2H, I). The nuclei of microvessel cells demonstrated strong expression of Ki-67 (Fig. 2J). These microvessels were not seen in adventitia of AAA. Real-time quantitative PCR analysis indicated that mRNA expression of VEGF-A, VEGF-C, and VEGFR-1, VEGFR-2, and VEGFR-3 was upregulated in AAA tissue, while that of VEGF-D was not significantly different, in comparison with expression levels in normal aortic tissues (Fig. 2K).

## Infiltration of inflammatory cells into AAA walls

Comparison between normal aorta and AAA walls revealed marked degradation of elastin fibers in the media (Fig. 3A, C). Immunohistochemical staining showed both nuclear and cytoplasmic expression of hypoxia-inducible factor (HIF)-1α in the intima/media of AAA walls (Fig. 3D), while HIF-1α expression was not detected in that of normal aorta (Fig. 3B). Double immunofluorescence staining demonstrated infiltration of CD11b-positive macrophages with strong nuclear/cytoplasmic expression of HIF-1α into the intima/media of AAA(Fig. 3E). Those macrophages with strong nuclear/cytoplasmic expression of HIF-1α also expressed VEGF-C and MMP-9 (Fig. 3F,G)

Using EVG and immunohistochemical staining of AAA walls, lymphatic microvessels were observed in the intima/media with degradation of elastin fibers (Fig. 4A,B). Inflammatory cells, such as macrophages, CD3-positive T lymphocytes, CD19-positive B lymphocytes, and neutrophils infiltrated in the surrounding intima/media andadventitia (Fig. 4C–F). Infiltration of these inflammatory cells was more prominent in the surrounding intima/media microvessels. Large macrophages were observed in the surrounding intima/media microvessels, while small macrophages were observed in the adventitia of AAA (Fig. 4G–M). Double immunofluorescence staining indicated that both types of macrophages (large macrophages in intima/media and small macrophages in adventitia) were positive for CD11b (Fig. 4G). However, only the large macrophages observed in the intima/media were positive for LYVE-1 (Fig. 4H). Similarly, large macrophages in the intima/media but not small macrophages in adventitia expressed VEGF-C, MMP-9, TGF-β1, IL-4, IL-8, MIP-1α, and MCP-1 (Fig. 4I, J, K, L, M, N, P). IFN-γ was not expressed either large macrophages in the intima/media or small macrophages in adventitia (Fig. 4P). CD3-positive T lymphocytes in the intima/media did not express either VEGF-C, MMP-9, IL-8, or MIP-1α, but expressed TGF-β1, IL-4, IFN-γ(Fig. 4Q).CD19-positive B lymphocytes and MPO-positive neutrophils in the intima/media did not express either VEGF-C, MMP-9, TGF-β1, IL-4, IL-8, MIP-1α, IFN-γ, and MCP-1(Fig. 4R,S).

## Lymph stasis in AAA walls

During open surgical repair of infra-renal AAA, ICG fluorescence lymphography was observed intraoperatively with a near-infrared camera after exposure of the retroperitoneal space to investigate lymph stasis, and strong ICG fluorescence signals were observed in the aneurysmal wall (Fig. 5 A–C). The pattern of the fluorescence-signal distribution was heterogeneous. ICG fluorescence lymphography was performed in all 17 patients with AAA. ICG fluorescence signals were identified in the AAA wall of all patients. Fluorescence lymphography of cross-sections of the aneurysmal wall in resected samples macroscopically localized the fluorescence signals to the intima/media area of the AAA wall (Fig. 5D–F). Near-infrared fluorescence microscopy also localized ICG fluorescence in the intima/media but not in adventitia,

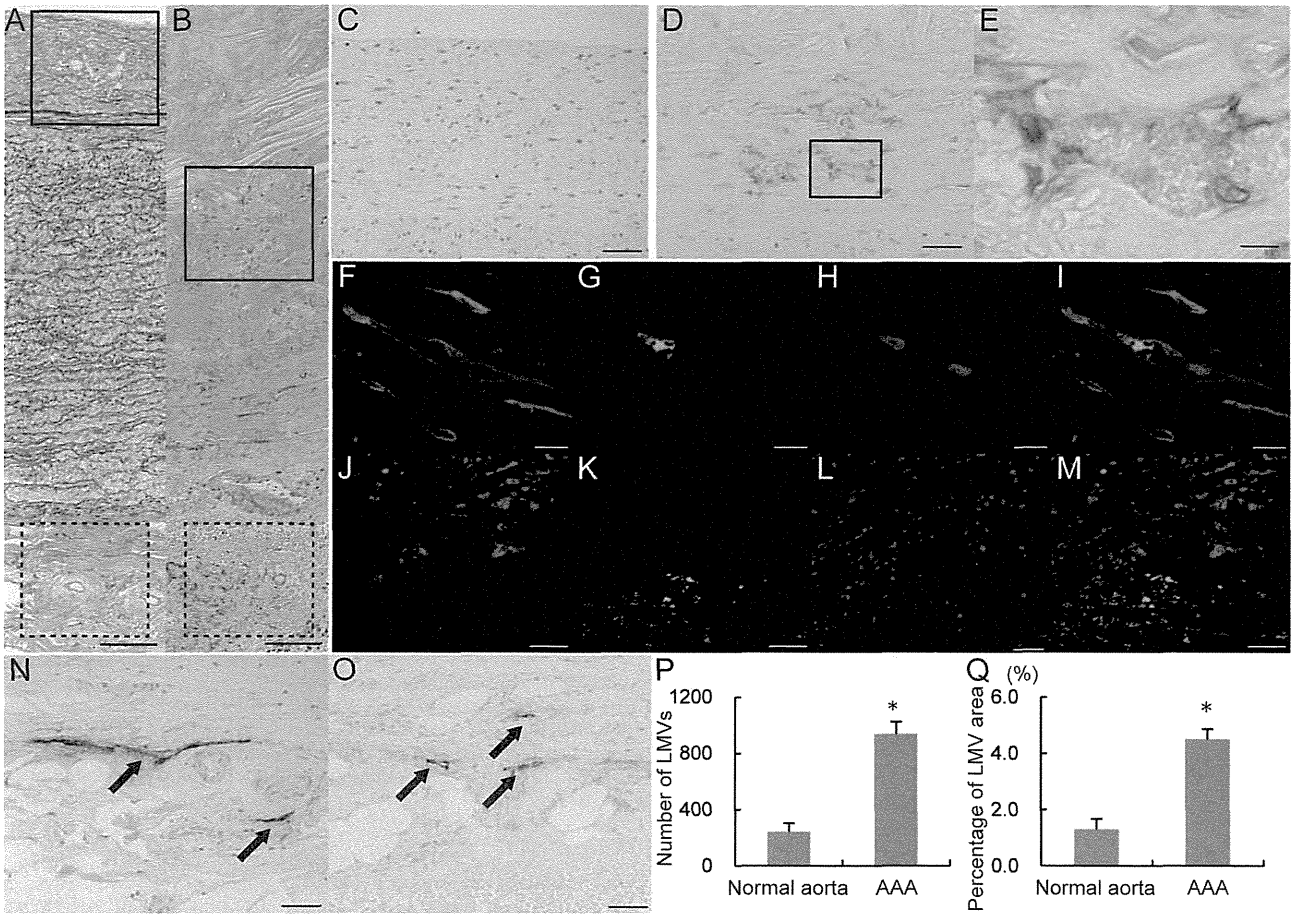


**Figure 1. Lymphatic microvessels in intima of abdominal aortic aneurysm.** EVG staining of normal aorta (**A**) and abdominal aortic aneurysm (AAA) wall (**B**). Immunohistochemistry for podoplanin corresponding to the areas outlined with a solid line in **A** and **B** (**C**, normal aorta; **D**, AAA). Podoplanin-positive microvessels were markedly increased in the intima in AAA wall. **E**, Higher magnification of the outlined area in **D**. Double immunofluorescence staining of lymphatic vessels in intima of AAA (**F–I**). **F**, Podoplanin (red); **G**, Prox-1 (green); **H**, DAPI (blue); **I**, merge of podoplanin, Prox-1, and DAPI. Double immunofluorescence staining of smooth muscle cells in intima of AAA (**J–M**). **J**, podoplanin (red); **K**, alpha smooth muscle isoform of actin (green), **L**, DAPI (blue); **M**, merge of podoplanin, alpha smooth muscle isoform of actin, and DAPI. Immunohistochemistry for podoplanin corresponding to the areas outlined with a dotted line in **A** and **B** (**N**; normal aorta, **O**; AAA). Lymphatic vasa vasorum was observed in adventitia in both normal aorta (**N**) and AAA (**O**) (black arrow: LVV). Scale bars indicate 100 μm (**A, B**), 50 μm (**C, D, J–M, N, O**), and 10 μm (**E–I**). Lymphatic microvessel density; the mean number of lymphatic microvessel (LMVs) in 10 microscopic fields at high magnification (×200) (**P**). Percentage of lymphatic microvessel area in 10 microscopic fields at high magnification (×200) (**Q**). Lymphatic microvessel density and percentage of lymphatic microvessel area were compared between normal aorta and AAA. (*$P<0.001$).
doi:10.1371/journal.pone.0089830.g001

suggesting that lymph stasis occurred in the intima/media (Fig. 5G, H). Immunohistochemical staining revealed both extensive infiltration of macrophages and the presence of lymphatic microvessels in the intima/media of the AAA wall with lymph stasis (Fig. 5I–L).

## Discussion

Lymph transportation network in aortic wall tissue is largely unknown. Recently, Drozdz et al. first reported the presence of adventitial LVV in human aorta with an immunohistological technique [19]. In the present study, we also demonstrated the presence of adventitial LVV in both autopsied normal aorta and AAA. There seemed to be no morphological differences in adventitial LVV in AAA. The LVV is an innate vascular structure for lymph transportation, although the detailed role of LVV in aortic tissue is yet to be identified. Immunohistological examination also revealed intimal/medial lymphangiogenesis in the AAA wall, particularly in the area where medial elastin was markedly degraded. While lymphatic vessels are usually absent from normal aortic intima and media, podoplanin-positive microvessels significantly increased in AAA intima/media. Podoplanin is specifically expressed by lymphatic endothelial cells but not blood vascular endothelial cells [20]. Podoplanin has also been reported in normal cells other than lymphatic endothelial cells, such as peritoneal mesothelial cells, osteocytes, glandular myoepithelial cells, ependymal cells, stromal reticular cells and follicular dendritic cells [21], and was observed in intimal smooth muscle cells in atherosclerotic aorta [22]. In the present study, podoplanin expression was seen in the intima/media of AAA, but not co-localized with smooth muscle cells. The nuclei of podoplanin-positive cells that formed vessels expressed Prox-1. Therefore, we speculated that the podoplanin-positive microvessels were lymphatic microvessels arising from lymphangiogenesis.

Lymphangiogenic factors such as VEGF-C and VEGFR-3 were also present in the areas in which podoplanin-positive microvessels were observed. CD11b-positive macrophages were observed